

Stable soliton dark matter wormhole in non-minimally coupled $f(\mathcal{Q}, \mathcal{T})$ gravity

G.G.L. Nashed * and Waleed El Hanafy †

Centre for Theoretical Physics, The British University in Egypt,
P.O. Box 43, El Sherouk City, Cairo 11837, Egypt

(Dated: June 13, 2025)

We show that non-minimal coupling between matter and geometry can indeed help in constructing stable, traversable, wormholes (WHs) without requiring exotic matter under certain conditions. In models like $f(\mathcal{Q}, \mathcal{T}) = \mathcal{Q} + \beta\mathcal{T}$ gravity, where \mathcal{Q} is the non-metricity scalar, and \mathcal{T} is the trace of the energy-momentum tensor, the coupling between matter and geometry introduces additional degrees of freedom in terms of the parameter β . These can mimic the effects of exotic matter or even replace it entirely under specific parameter choice. The analysis involves deriving WH shape functions based on two dark matter (DM) density profiles: a solitonic core at the center of DM halos, and the outer halo follows the universal Navarro-Frenk-White (NFW) density profile of cold DM (CDM). The wormhole solutions derived in these models satisfy important geometric conditions like: Flaring-out condition (necessary for traversability) and asymptotic flatness condition. For large positive coupling parameter, the null energy condition (NEC) can be satisfied at the wormhole throat, meaning exotic matter is not needed, while the wormhole is no longer Lorentzian and the flaring-out condition is broken. However, for large negative coupling parameter, the NEC can be satisfied, allowing for healthy wormholes without exotic matter, provided the coupling strength remains within certain bounds. In the latter case, the NEC is broken only effectively. We investigate the stability of the obtained wormhole solutions by virtue of a modified version of Tolman–Oppenheimer–Volkoff (TOV) equation, which includes a new force due to matter-geometry non-minimal, showing that these wormholes can be dynamically stable.

I. INTRODUCTION

Current cutting-edge studies in astrophysics and cosmology are propelling us towards a fresh phase of revelations concerning the Universe. Partnerships like the collaboration of LIGO [1], EHT [2, 3], INTEGRAL [4], Virgo [5], ATHENA [6], IXPE [7], Swift [8], as well as CHIME [9] are conducting unprecedented experiments on gravity and astrophysical objects. Additionally, upcoming investigations of BINGO [10], SKA [11] and LISA [12] could significantly limit the scope of gravity theories, narrowing down the plethora of theoretical ideas circulating in academic literature.

The wormhole is a fascinating and unusual solution to Einstein's equations in general relativity [13]. The wormhole serves as a topological connection between points in separate universes or within the same universe. Although it could be considered as a theoretical concept, numerous studies have been conducted on the possibility of discovering wormholes. In the study carried out by Bueno et al. (2018) [14] an intriguing method was suggested to locate detectable wormholes by utilizing gravitational wave data to analyze echoes of the gravitational wave signal near black hole horizons to improve the sentence flow. The rings produced after a merger are associated with the emission of gravitational waves during the post-merger phase of binary mergers. Additionally, Paul et al. [15] examined unique features of accretion disk images to differentiate a wormhole shape from a black hole, putting forward an alternative fascinating opportunity for observation. Furthermore, extensive research has been conducted on the gravitational lensing caused by a wormhole and the deflection of light [16–18].

Another sought-after aspect regarding wormholes is the quest for traversable options - that is, wormholes that are sufficiently large for a person to pass through and withstand the powerful tidal forces. Morris and Thorne's groundbreaking paper [19] first introduced this type of wormholes, which remains a popular topic, evident in the impressive research presented in [20]. In their study [20] authors introduced a novel dark sector in the Randall–Sundrum model [21] with a $U(1)$ gauge field which only interacts with particles in the standard model through the force of gravity, allowing for the potential existence of traversable wormholes. Wormhole has been investigated within modified gravity, it has been shown that traversable wormholes can be constructed within in $f(G)$ modified gravity, where G denotes the Gauss–Bonnet term, for anisotropic, isotropic and barotropic fluids cases [22].

Up to now, general relativity remains the prevailing explanation supported by many for its gravitational force influence through observations and experiments. Nevertheless, certain events that are governed by general relativity fails to fully explain, like the accelerated cosmic expansion, the gravitation at galactic scales, as well as the search

* nashed@bue.edu.eg

† waleed.elhanafy@bue.edu.eg

for a quantum theory to describe gravity. Alternative explanations for these issues have been suggested in the form of different gravity theories. These theories make alterations or expansions to general relativity in different manners. An example of extending general relativity is $f(\mathcal{R})$ gravitational theory. Modifying the Einstein-Hilbert action, this theory is changed by substituting a function of the scalar curvature for the Ricci scalar [23–29]. This alteration results in modifications to the equations governing the gravitational field, potentially impacting how gravity acts on various scales. This theory explains the speeding up of the Universe's expansion, supports limits on early inflation, and removes the necessity of DM to account for galaxy rotation, star movement, and galaxy shape [30].

In the year 2011, Harko and colleagues [31] presented a modified version of $f(\mathcal{R})$ known as $f(\mathcal{R}, \mathcal{T})$ gravitational theory. Such a theory adds an additional factor to Einstein's equations based on the energy-momentum tensor trace. This contribution would explain the typical display of significant quantum phenomena related to features of conformal anomaly within $f(\mathcal{R}, \mathcal{T})$ modified gravity. The theory has undergone testing using various realistic and conceptual methods as evident in [32–35].

In addition to prior general relativity extensions, we emphasize the $f(\mathcal{Q})$ gravitational theory proposed by Jimenez and colleagues [36]. This theory posits that gravitational interaction is caused by the non-metricity scalar \mathcal{Q} . In recent years, various observational data have been used to test the $f(\mathcal{Q})$ gravity theory, as demonstrated in the research conducted by Lazkoz et al. [37]. The researchers used information from the growth rate, Gamma-Ray Bursts, Type Ia Supernovae, Cosmic Microwave Background, Quasars, Baryon Acoustic Oscillations data and in order to constrain $f(\mathcal{Q})$ gravity. Furthermore, the impact of viscosity on cosmic acceleration has been examined within the framework of $f(\mathcal{Q})$ gravity [38, 39]. Furthermore, Mandal et al. confirmed the appropriateness of $f(\mathcal{Q})$ in the domain of cosmology using the energy conditions [40]. In their study [40], the researchers presented the embedding procedure, allowing for the incorporation of complex aspects from the absence of metricity in the energy requirement. A recent research showed that $f(\mathcal{Q})$ gravity has been effectively utilized in both Casimir wormholes and the GUP-corrected Casimir wormhole [41, 42].

Xu et al. [43] expanded the $f(\mathcal{Q})$ gravity to include $f(\mathcal{Q}, \mathcal{T})$ gravity, with \mathcal{T} representing the energy-momentum tensor trace. This trace is in charge of including additional quantum realm's contributions to traditional gravity. Arora et al. recently demonstrated the feasibility of the theory of gravitation of $f(\mathcal{Q}, \mathcal{T})$ in the domain of cosmology in relation to energy requirements [44], while Tayde et al. [45] employed the matching condition to exam the stability of a slender shell encasing the wormhole and the potential it generates.

During our study, we thoroughly analyze a specific $f(\mathcal{Q}, \mathcal{T}) \equiv \mathcal{Q} + \beta\mathcal{T}$ theory, where the wormhole models are computed by employing fuzzy dark matter which includes soliton quantum wave DM at the core of the halo while the outer regions follow NFW parameterization of the CDM. The ideas covered in this research are delineated in the subsequent sections as follows: In Sec. II, we provided an overview of the $f(\mathcal{Q}, \mathcal{T})$ gravity theory. In Sec. III, we discuss Morris-Thorne spacetime which describes wormhole models and the corresponding traversability conditions. We apply the field equations of $f(\mathcal{Q}, \mathcal{T})$ theory to the Morris-Thorne spacetime and their consequence on the energy conditions, with a particular focus on the linear $f(\mathcal{Q}, \mathcal{T}) \equiv \mathcal{Q} + \beta\mathcal{T}$ theory. In Sec. IV, we present the matter, assumed to fill the wormhole, in this study. We discuss two density profiles corresponds to Soliton+NFW, where solitons quantum wave DM at the core of dwarf galaxies and the outer regions follow the NFW density profile which characterizes the CDM. In Sec. V, we derive the wormhole shape functions correspond to the two density profiles assumed in the present study. We investigate possible constraints on the coupling parameter β from traversability conditions of wormhole geometry. In Sec. VI, we investigate additional possible constraints on the coupling parameter β from the modified energy conditions corresponds to the linear $f(\mathcal{Q}, \mathcal{T})$ gravity. In Sec. VII, we study the stability of the obtained wormhole solutions via a modified version of the TOV equation of hydrostatic equilibrium. The final section is devoted to summarize the results presented in this study and future work.

II. BASES OF $f(\mathcal{Q}, \mathcal{T})$ GRAVITATIONAL THEORY

In this section, we provide the main characteristics of a general $f(\mathcal{Q}, \mathcal{T})$ theory. We write the action [43]

$$\mathcal{S} = \int \frac{1}{2\kappa^2} f(\mathcal{Q}, \mathcal{T}) \sqrt{-g} d^4x + \int \mathcal{L}_m \sqrt{-g} d^4x, \quad (1)$$

where $\kappa^2 = 8\pi G/c^4$, with G being the gravitational constant and c is the speed of light, g denotes the determinant of the metric tensor $g_{\mu\nu}$ and \mathcal{L}_m is the matter Lagrangian density. The scalar \mathcal{Q} is related to the non-metricity tensor,

$$\mathcal{Q}_{\lambda\mu\nu} = \nabla_\lambda g_{\mu\nu}, \quad (2)$$

by the following relation [36]

$$\mathcal{Q} = -\mathcal{Q}_{\alpha\mu\nu} P^{\alpha\mu\nu} \equiv -g^{\mu\nu} \left(L^\beta_{\alpha\mu} L^\alpha_{\nu\beta} - L^\beta_{\alpha\beta} L^\alpha_{\mu\nu} \right). \quad (3)$$

The tensor P is commonly referred to as the superpotential tensor

$$P^\alpha_{\mu\nu} = \frac{1}{4} \left[2\mathcal{Q}_{(\mu}{}^\alpha_{\nu)} - \mathcal{Q}^\alpha_{\mu\nu} + \mathcal{Q}^\alpha g_{\mu\nu} - \tilde{\mathcal{Q}}^\alpha g_{\mu\nu} - \delta^\alpha_{(\mu} \mathcal{Q}_{\nu)} \right], \quad (4)$$

and the tensor L is known as disformation tensor

$$L^\beta_{\mu\nu} = \frac{1}{2} \mathcal{Q}^\beta_{\mu\nu} - \mathcal{Q}_{(\mu}{}^\beta_{\nu)}. \quad (5)$$

In the above expressions, we used

$$\mathcal{Q}_\alpha = \mathcal{Q}_\alpha{}^\mu_\mu, \quad \tilde{\mathcal{Q}}_\alpha = \mathcal{Q}^\mu{}_{\alpha\mu}. \quad (6)$$

The variation of the action (1) with respect to the metric tensor $g_{\mu\nu}$ gives the following field equations of $f(\mathcal{Q}, \mathcal{T})$ modified gravity as [43, 44]:

$$\frac{-2}{\sqrt{-g}} \nabla_\alpha (\sqrt{-g} f_{\mathcal{Q}} P^\alpha_{\mu\nu}) - \frac{1}{2} g_{\mu\nu} f + f_{\mathcal{T}} (\mathcal{T}_{\mu\nu} + \Theta_{\mu\nu}) - f_{\mathcal{Q}} (P_{\mu\alpha\beta} \mathcal{Q}_\nu{}^{\alpha\beta} - 2 \mathcal{Q}^{\alpha\beta}{}_\mu P_{\alpha\beta\nu}) = \kappa^2 \mathcal{T}_{\mu\nu}. \quad (7)$$

Here $f_{\mathcal{Q}}$ refers to $f_{\mathcal{Q}} = \frac{\partial f}{\partial \mathcal{Q}}$ and $f_{\mathcal{T}} = \frac{\partial f}{\partial \mathcal{T}}$. Additionally, the tensors $\Theta_{\mu\nu}$ and $\mathcal{T}_{\mu\nu}$ are defined as:

$$\Theta_{\mu\nu} = g^{\alpha\beta} \frac{\delta \mathcal{T}_{\alpha\beta}}{\delta g^{\mu\nu}}, \quad \mathcal{T}_{\mu\nu} = -\frac{2}{\sqrt{-g}} \frac{\delta (\sqrt{-g} \mathcal{L}_m)}{\delta g^{\mu\nu}}. \quad (8)$$

Remarkably $f(\mathcal{Q}, \mathcal{T})$ gravity theory has attracted interest in the last few years from several aspects. In cosmological applications, it has been shown that the theory can account for late accelerated expansion without the need for dark energy [46]. Viability of $f(\mathcal{Q}, \mathcal{T})$ gravity has been tested with cosmological observations [47]. On the other hand, in the realm of astrophysics, stability of compact stellar models within $f(\mathcal{Q}, \mathcal{T})$ gravity have been investigated, where a compact star heavier than the GR predictions can be obtained [48]. Additionally, the impact of anisotropic matter and electromagnetism on the compactness and sound speed limits, within stars, has been studied [49, 50].

III. STUDY OF WORMHOLES IN $f(\mathcal{Q}, \mathcal{T})$ GRAVITATIONAL THEORY

In this section, we discuss two unknown functions which characterize wormhole solutions, those are the redshift and the shape functions. Additionally, we discuss the constraints which govern those functions in order to obtain a traversable wormhole. Next, we derive the corresponding field equations of a general $f(\mathcal{Q}, \mathcal{T})$ form in presence of anisotropic fluid. We show possible implications of $f(\mathcal{Q}, \mathcal{T})$ modifications on the energy conditions which play essential roles in wormhole solutions. Finally, we discuss a particular theory with linear behavior, i.e. $f(\mathcal{Q}, \mathcal{T}) = \mathcal{Q} + \beta \mathcal{T}$, which represents a simple case of non-minimal coupling between matter and geometry.

A. Traversable wormhole spacetime configuration

To discuss the general aspects of wormhole models in $f(\mathcal{Q}, \mathcal{T})$ theory, we will examine a spherically symmetric wormhole metric. This analysis follows the influential researches presented in [13, 19], where the line element is considered as the Morris-Thorne wormhole metric

$$ds^2 = e^{2\xi(r)} dt^2 - \left(1 - \frac{h(r)}{r} \right)^{-1} dr^2 - r^2 d\theta^2 - r^2 \sin^2 \theta d\Phi^2. \quad (9)$$

Here $h(r)$ and $\xi(r)$ represent the shape and redshift functions, respectively. We believe that the models of wormhole in $f(\mathcal{Q}, \mathcal{T})$ can be consistent within Birkhoff's theorem because the line element (9) is presented in polar form (t, r, θ, Φ) . The hypothesis about the applicability of Birkhoff's theorem is supported by the study presented in [51] as well as the recent review by Bahamond et al. [52]. The relevance of the Birkhoff theorem in the realm of teleparallel gravity was discussed in [51]. Short time ago, Bahamonde et al. assessed the relevance of Birkhoff's theorem in an extended version of teleparallel gravity, including influences from a boundary term and scalar fields. In their study [52], they demonstrated that Birkhoff's theorem is limited solely if the scalar fields are based on the variables t or r coordinate. In Eq. (5.49) presented in [52], the authors demonstrated a mapping correlation between the non-metricity and torsion scalars. This correlation, combined with the considerations of Birkhoff's theorem in the frame of teleparallel theory,

backs up the hypothesis about the applicability of this theorem for spherically symmetric solutions within $f(\mathcal{Q}, \mathcal{T})$ theory.

When looking for a traversable wormhole model, specific conditions on the redshift and shape function must be fulfilled [13, 19]:

- (i) In general the shape function $h(r) < r$, whereas $h(r_0) = r_0$ at a minimal radius (the wormhole throat), known as the throat condition.
- (ii) The function $h(r)$ must satisfy the flaring out condition $\frac{h-rh'}{2h^2} > 0$, where $h'(r_0) < 1$ at the wormhole throat.
- (iii) The wormhole must be asymptotically flat condition, i.e. the ratio $\frac{h(r)}{r} \rightarrow 0$ as $r \rightarrow \infty$.
- (iv) The redshift function $\xi(r)$ must have a finite value at all points.

B. The field equations

In this study, we consider that the matter of wormhole solutions is defined by a non-uniform energy-momentum tensor supplied by:

$$T_\mu^\nu = (\sigma c^2 + p_\theta) U_\mu U^\nu - p_\theta \delta_\mu^\nu + (p_r - p_\theta) V_\mu V^\nu. \quad (10)$$

The vectors U_μ and V_μ denote the 4-velocity vector and space-like unit vector, where $U_\mu U^\nu = -V_\mu V^\nu = 1$. In addition, the energy density, σ , the radial pressure, p_r , and the tangential pressure, p_θ , all are functions of the radial coordinate r . The trace of the stress-energy tensor (10) is given as follows $T = \sigma c^2 - p_r - 2p_\theta$. We note that Letelier introduced the anisotropic energy-momentum tensor as a means to explore a theoretical framework in plasma physics that deals with two distinct fluids [53]. Additionally, it has been used in a variety of scenarios to mimic magnetized neutron stars [54].

Now we are ready to replicate the methods used in [55] to discover solutions with static wormhole in $f(\mathcal{Q}, \mathcal{T})$. In this study we choose $\mathcal{L}_m = -P$, where the average pressure $P \equiv \frac{p_r + 2p_\theta}{3}$. This Lagrangian reads Eq. (8) as follows

$$\Theta_{\mu\nu} = -g_{\mu\nu} P - 2T_{\mu\nu}. \quad (11)$$

Furthermore, for the spacetime metric (9), the scalar \mathcal{Q} is explicitly expressed as [56]

$$\mathcal{Q} = -\frac{h}{r^2} \left[\frac{rh' - h}{r(r-h)} + 2\xi' \right]. \quad (12)$$

By virtue of Eqs. (10) and (12), we write the field equations (7) as follows [57]

$$\frac{2(r-h)}{(2r-h)f_\mathcal{Q}} \left[\sigma c^2 - \frac{(r-h)}{\kappa^2 r^3} \left(\frac{hrf_{\mathcal{Q}\mathcal{Q}}\mathcal{Q}'}{r-h} + hf_\mathcal{Q} \left(\frac{r\xi' + 1}{r-h} - \frac{2r-h}{2(r-h)^2} \right) + \frac{fr^3}{2(r-h)} \right) + \frac{f_\mathcal{T}(P+\sigma)}{\kappa^2} \right] = \frac{h'}{\kappa^2 r^2}, \quad (13)$$

$$\begin{aligned} & \frac{2h}{fr^3} \left[p_r + \frac{(r-h)}{2\kappa^2 r^3} \left(f_\mathcal{Q} \left(\frac{h \left(\frac{rh'-h}{r-h} + 2r\xi' + 2 \right)}{r-h} - 4rh' \right) + \frac{2hrf_{\mathcal{Q}\mathcal{Q}}\mathcal{Q}'}{r-h} \right) + \frac{fr^3(r-h)\xi'}{\kappa^2 hr^2} - \frac{f_\mathcal{T}(P-p_r)}{\kappa^2} \right] \\ &= \frac{1}{\kappa^2} \left[2 \left(1 - \frac{h}{r} \right) \frac{\xi'}{r} - \frac{h}{r^3} \right], \end{aligned} \quad (14)$$

$$\begin{aligned} & \frac{1}{f_\mathcal{Q} \left(\frac{r}{r-h} + r\xi' \right)} \left[p_\theta + \frac{(r-h)}{4\kappa^2 r^2} \left(f_\mathcal{Q} \left(\frac{4(2h-r)\xi'}{r-h} - 4r(\xi')^2 - 4r\xi'' \right) + \frac{2fr^2}{r-h} - 4rf_{\mathcal{Q}\mathcal{Q}}\mathcal{Q}'\xi' \right) - \frac{f_\mathcal{T}(P-p_\theta)}{\kappa^2} \right. \\ & \left. + \frac{(r-h)}{\kappa^2 r} \left(\xi'' + \xi'^2 - \frac{(rh'-h)\xi'}{2r(r-h)} + \frac{\xi'}{r} \right) f_\mathcal{Q} \left(\frac{r}{r-h} + r\xi' \right) \right] = \frac{1}{\kappa^2} \left(1 - \frac{h}{r} \right) \left[\xi'' + \xi'^2 - \frac{(rh'-h)\xi'}{2r(r-h)} - \frac{rh'-h}{2r^2(r-h)} + \frac{\xi'}{r} \right]. \end{aligned} \quad (15)$$

The above equations are the non-vanishing components of the equations of motion of $f(\mathcal{Q}, \mathcal{T})$ theory [56]. It is straightforward to show that the above field equations can alternatively written in the form

$$\kappa^2 \sigma c^2 = \frac{(r-h)}{2r^3} \left[f_\mathcal{Q} \left\{ \frac{(2r-h)(rh'-h)}{(r-h)^2} + \frac{h(2r\xi' + 2)}{r-h} \right\} + \frac{2hrf_{\mathcal{Q}\mathcal{Q}}\mathcal{Q}'}{r-h} + \frac{fr^3}{r-h} - \frac{2r^3 f_\mathcal{T}(P+\sigma c^2)}{(r-h)} \right], \quad (16)$$

$$\kappa^2 p_r = -\frac{(r-h)}{2r^3} \left[f_{\mathcal{Q}} \left\{ \frac{h}{r-h} \left(\frac{rh'-h}{r-b} + 2r\xi' + 2 \right) - 4r\xi' \right\} + \frac{2hrf_{\mathcal{Q}}\mathcal{Q}'}{r-h} + \frac{fr^3}{r-h} - \frac{2r^3f_{\mathcal{T}}(P-p_r)}{(r-h)} \right], \quad (17)$$

$$\kappa^2 p_{\theta} = -\frac{(r-h)}{4r^2} \left[f_{\mathcal{Q}} \left\{ \frac{(rh'-h) \left(\frac{2r}{r-h} + 2r\xi' \right)}{r(r-h)} + \frac{4(2h-r)\xi'}{r-h} - 4r\xi'^2 - 4r\xi'' \right\} - 4rf_{\mathcal{Q}}\mathcal{Q}'\xi' + \frac{2fr^2}{r-h} - \frac{4r^2f_{\mathcal{T}}(P-p_{\theta})}{(r-h)} \right]. \quad (18)$$

To adequately ascertain the limits of σ , p_r and p_{θ} , one could write the field equations for traversable wormholes in GR like-frame, which yields

$$G_{\mu\nu} = \kappa^2 (\mathcal{T}_{\mu\nu} + \mathcal{T}_{\mu\nu}^{\text{NMG}}) = \kappa^2 \tilde{\mathcal{T}}_{\mu\nu}, \quad (19)$$

where $\mathcal{T}_{\mu\nu}^{\text{NMG}}$ denotes the non-minimal coupling between matter and gravity, while $\tilde{\mathcal{T}}_{\mu\nu}$ denotes the effective (total) stress-energy tensor, i.e. $\tilde{\mathcal{T}}^{\mu}_{\nu} = \text{diag}(\tilde{\sigma}c^2, \tilde{p}_r, \tilde{p}_{\theta}, \tilde{p}_{\theta})$. Therefore, we write

$$\tilde{\sigma}c^2 = \frac{h'}{\kappa^2 r^2}, \quad (20)$$

$$\tilde{p}_r = \frac{1}{\kappa^2} \left[2 \left(1 - \frac{h}{r} \right) \frac{\xi'}{r} - \frac{h}{r^3} \right], \quad (21)$$

$$\tilde{p}_{\theta} = \frac{1}{\kappa^2} \left(1 - \frac{h}{r} \right) \left[\xi'' + \xi'^2 - \frac{(rh'-h)\xi'}{2r(r-h)} - \frac{rh'-h}{2r^2(r-h)} + \frac{\xi'}{r} \right]. \quad (22)$$

Here $\tilde{\sigma}$, \tilde{p}_r and \tilde{p}_{θ} represent the effective density, radial and tangential pressures. The above equations show that the solution for the effective sector is nothing but the GR one. It proves convenient to write the effective fluid in terms of the matter fluid including the effects due to non-minimal coupling between gravity and matter. This shows how the matter sector in modified gravity is different from the GR framework. The comparison between the set of equations (13)-(15) and Eqs. (20)-(22) enables us to obtain the following important relations [57]

$$\tilde{\sigma}c^2 = \frac{2(r-h)}{(2r-h)f_{\mathcal{Q}}} \left[\sigma c^2 - \frac{1}{\kappa^2 r^2} \left(1 - \frac{h}{r} \right) \left(\frac{hrf_{\mathcal{Q}}\mathcal{Q}'}{r-b} + hf_{\mathcal{Q}} \left(\frac{r\xi' + 1}{r-h} - \frac{2r-h}{2(r-h)^2} \right) + \frac{fr^3}{2(r-h)} \right) + \frac{f_{\mathcal{T}}(P+\sigma c^2)}{\kappa^2} \right], \quad (23)$$

$$\tilde{p}_r = \frac{2h}{fr^3} \left[p_r + \frac{1}{2\kappa^2 r^2} \left(1 - \frac{h}{r} \right) \left(f_{\mathcal{Q}} \left(\frac{h \left(\frac{rh'-h}{r-h} + 2r\xi' + 2 \right)}{r-h} - 4r\xi' \right) + \frac{2hrf_{\mathcal{Q}}\mathcal{Q}h'}{r-g} \right) + \frac{fr^3(r-h)\xi'}{\kappa^2 hr^2} - \frac{f_{\mathcal{T}}(P-p_r)}{\kappa^2} \right], \quad (24)$$

$$\begin{aligned} \tilde{p}_{\theta} = & \frac{1}{f_{\mathcal{Q}} \left(\frac{r}{r-h} + r\xi' \right)} \left[p_{\theta} + \frac{1}{4\kappa^2 r} \left(1 - \frac{h}{r} \right) \left(f_{\mathcal{Q}} \left(\frac{4(2h-r)\xi'}{r-h} - 4r(\xi')^2 - 4r\xi'' \right) + \frac{2fr^2}{r-h} - 4rf_{\mathcal{Q}}\mathcal{Q}'\xi' \right) \right. \\ & \left. + \frac{1}{\kappa^2} \left(1 - \frac{h}{r} \right) \left(\xi'' + \xi'^2 - \frac{(rh'-h)\xi'}{2r(r-h)} + \frac{\xi'}{r} \right) f_{\mathcal{Q}} \left(\frac{r}{r-h} + r\xi' \right) - \frac{f_{\mathcal{T}}(P-p_{\theta})}{\kappa^2} \right]. \end{aligned} \quad (25)$$

C. The energy conditions of wormhole with constant redshift in $f(\mathcal{Q}, \mathcal{T})$ gravity

For a constant redshift function $\xi(r) = \xi_0$, the effective density and pressures read

$$\tilde{\sigma}c^2 = \frac{2(r-h)}{(2r-h)f_{\mathcal{Q}}} \left[\sigma c^2 - \frac{\left(1 - \frac{h}{r} \right) \left\{ \frac{hrf_{\mathcal{Q}}\mathcal{Q}'}{r-h} + \frac{hf_{\mathcal{Q}}}{r-h} - \frac{h(2r-h)f_{\mathcal{Q}}}{2(r-h)^2} + \frac{fr^3}{2(r-h)} \right\}}{\kappa^2 r^2} + \frac{f_{\mathcal{T}}(P+\sigma c^2)}{\kappa^2} \right], \quad (26)$$

$$\tilde{p}_r = \frac{2h}{fr^3} \left[p_r - \frac{f_{\mathcal{T}}(P-p_r)}{\kappa^2} + \frac{\left(1 - \frac{h}{r} \right) \left\{ \frac{hf_{\mathcal{Q}} \left(\frac{rh'-h}{r-b} + 2 \right)}{r-h} + \frac{2hrf_{\mathcal{Q}}\mathcal{Q}'}{r-h} \right\}}{2\kappa^2 r^2} \right], \quad (27)$$

$$\tilde{p}_\theta = \frac{(r-h)}{rf_Q} \left[p_\theta - \frac{f_T(P-p_\theta)}{\kappa^2} + \frac{fr(1-\frac{h}{r})}{2\kappa^2(r-h)} \right]. \quad (28)$$

A couple of lines will be devoted to standard energy conditions, which are based on the Raychaudhuri equations. These equations allow one to explain how gravity affects the convergence and divergence of time-like, spacelike, and light-like curves. The Raychaudhuri equations establish limitations on the density and pressures of a wormhole, described by Arora et al. [44] as:

- The weak energy condition (WEC) is satisfied whenever $\tilde{\sigma} \geq 0$ and $\tilde{\sigma}c^2 + \tilde{p}_j \geq 0 \forall j$ with $j = r$ or θ .
- If the sum of the energy density and pressure in all directions is non-negative, then the Null energy condition (NEC) holds.
- If $\tilde{\sigma} \geq 0$ and $\tilde{\sigma}c^2 - |\tilde{p}_j| \geq 0 \forall j$ with $j = r$ or θ , then the Dominant energy condition (DEC) is satisfied.
- Strong energy condition (SEC) is satisfied whenever $\tilde{\sigma}c^2 + \tilde{p}_r \geq 0$, $\tilde{\sigma}c^2 + \tilde{p}_\theta \geq 0$ and $\tilde{\sigma}c^2 + \tilde{p}_r + \tilde{p}_\theta \geq 0$.

Therefore, by considering the effective density and pressures as indicated in Eqs. (26)–(28), we obtain [57]:

$$\begin{aligned} \tilde{\sigma}c^2 + \tilde{p}_r = & \frac{h(h-2r)f_Q^2[h(3h-2r)-hrh']-fr^4(h-r)^2[2hf_{QQ}Q'+r^2\{f-2f_T(P+\sigma c^2)+2\kappa^2p_r\}]}{\kappa^2fr^6(h-2r)(h-r)f_Q} \\ & + \frac{2(r-h)(\sigma c^2+p_r)}{(2r-h)f_Q} + \frac{hr(h-r)f_Q[2(h-2r)\{Qf_{QQ}Q'+r^2(f_T(p_r-P)+\kappa^2p_r)\}-hfr^2]}{\kappa^2fr^6(h-2r)(h-r)f_Q}, \end{aligned} \quad (29)$$

$$\tilde{\sigma}c^2 + \tilde{p}_\theta = \frac{2(r-h)(\sigma+p_\theta)}{(2r-h)f_Q} - \frac{2h^2f_Q+r(r-h)[2rf_T(+2\sigma r-hp_\theta+hP+2rp_\theta)-h(4f_{QQ}Q'+fr+2\kappa^2rp_\theta)]}{2\kappa^2r^3(h-2r)f_Q}, \quad (30)$$

$$\begin{aligned} \tilde{\sigma}c^2 - \tilde{p}_r = & -\frac{h(h-2r)f_Q^2(h(3h-2r)-hrh')+fr^4(h-r)^2[2hf_{QQ}Q'+r^2\{f-2f_T(P+\sigma)-2\kappa^2p_r\}]}{\kappa^2fr^6(h-2r)(h-r)f_Q} \\ & + \frac{2(r-h)(\sigma-p_r)}{(2r-h)f_Q} - \frac{hr(h-r)f_Q[2(h-2r)\{hf_{QQ}Q'+r^2(f_T(p_r-P)+\kappa^2p_r)\}+hfr^2]}{\kappa^2fr^6(h-2r)(h-r)f_Q}, \end{aligned} \quad (31)$$

$$\tilde{\sigma}c^2 - \tilde{p}_\theta = \frac{2(r-h)(\sigma-p_\theta)}{(2r-h)f_Q} - \frac{2h^2f_Q+r(r-h)[2\{rf_T((h-2r)p_\theta-hP+4Pr+2\sigma r)-2bf_{QQ}Q'+\kappa^2hrp_\theta\}+fr(h-4r)]}{2\kappa^2r^3(h-2r)f_Q}, \quad (32)$$

$$\begin{aligned} \tilde{\sigma}c^2 + \tilde{p}_r + 2\tilde{p}_\theta = & +\frac{2(r-h)(p_r+2p_\theta+\sigma)}{(2r-h)f_Q} + \frac{hr}{\kappa^2r^6} \left[\frac{2(hf_{QQ}Q'+r^2\{f_T(p_r-P)+\kappa^2p_r\})}{f} - \frac{hr^2}{h-2r} \right] \\ & + \frac{h^2f_Q(3h-rh'-2r)}{\kappa^2r^6f(h-r)} + \frac{r^4(h-r)[2rf_T(hP-(h-2r)p_\theta-Pr+\sigma r)-2hf_{QQ}Q'+fr(r-h)-2\kappa^2r(hp_\theta+rp_r)]}{\kappa^2r^6(h-2r)f_Q}. \end{aligned} \quad (33)$$

Hence, the energy condition requirements for a wormhole model within $f(Q, T)$ theory, using the previously mentioned equations, lead to the following important results which relate the energy conditions on the matter sector and the effective sector [57].

- $\tilde{\sigma} \geq 0 \Rightarrow \sigma \geq 0$, where

$$\frac{(2r-h)f_Q}{r-h} > 0 \text{ and } \frac{2(r-h)}{(2r-h)f_Q} \left[\frac{\left(1-\frac{h}{r}\right)\left(\frac{hrf_{QQ}Q'}{r-h}+\frac{hf_Q}{r-h}-\frac{h(2r-h)f_Q}{2(r-h)^2}+\frac{fr^3}{2(r-h)}\right)}{\kappa^2r^2} - \frac{f_T(P+\sigma)}{\kappa^2} \right] \leq 0.$$

- $\tilde{\sigma} + \tilde{p}_r \geq 0 \Rightarrow \sigma + p_r \geq 0$, where

$$\begin{aligned} \frac{(2r-h)f_Q}{r-h} > 0 \text{ and } \frac{hr(h-r)f_Q[2(h-2r)(hf_{QQ}Q'+r^2(f_T(p_r-P)+\kappa^2p_r))-bfr^2]}{\kappa^2fr^6(b-2r)(b-r)f_Q} \\ & + \frac{h(h-2r)f_Q^2(h(3h-2r)-hrh')-fr^4(h-r)^2[2hf_{QQ}Q'+r^2(-2f_T(P+\sigma)+f+2\kappa^2p_r)]}{\kappa^2fr^6(h-2r)(h-r)f_Q} \geq 0. \end{aligned}$$

- $\tilde{\sigma} + \tilde{p}_\theta \geq 0 \Rightarrow \sigma + p_\theta \geq 0$, where

$$\frac{(2r-h)f_{\mathcal{Q}}}{r-h} > 0 \text{ and } \frac{2h^2f_{\mathcal{Q}} + r(r-h)[2rf_{\mathcal{Q}}(-hp_\theta + hP + 2rp_\theta + 2\sigma r) - h(4f_{\mathcal{Q}}\mathcal{Q}' + fr + 2\kappa^2rp_\theta)]}{2\kappa^2r^3(h-2r)f_{\mathcal{Q}}} \leq 0.$$

- $\tilde{\sigma} - \tilde{p}_r \geq 0 \Rightarrow \sigma - p_r \geq 0$, where

$$\begin{aligned} \frac{(2r-h)f_{\mathcal{Q}}}{r-h} &> 0 \text{ and } \frac{hr(h-r)f_{\mathcal{Q}}[2(h-2r)\{hf_{\mathcal{Q}}\mathcal{Q}' + r^2(f_{\mathcal{T}}(p_r - P) + \kappa^2p_r)\} + bfr^2]}{\kappa^2fr^6(b-2r)(b-r)f_{\mathcal{Q}}} \\ &+ \frac{h(h-2r)f_{\mathcal{Q}}^2[h(3h-2r) - hrh'] + fr^4(h-r)^2[2hf_{\mathcal{Q}}\mathcal{Q}' + r^2(-2f_{\mathcal{T}}(P + \sigma) + f - 2\kappa^2p_r)]}{\kappa^2fr^6(b-2r)(h-r)f_{\mathcal{Q}}} \leq 0. \end{aligned}$$

- $\tilde{\sigma} - \tilde{p}_\theta \geq 0 \Rightarrow \sigma - p_\theta \geq 0$, where

$$\frac{(2r-h)f_{\mathcal{Q}}}{r-h} > 0 \text{ and } \frac{2h^2f_{\mathcal{Q}} + r(r-h)[2(rf_{\mathcal{T}}((h-2r)p_\theta - hP + 4Pr + 2\sigma r) - 2bf_{\mathcal{Q}}\mathcal{Q}' + \kappa^2hrp_\theta) + fr(h-4r)]}{2\kappa^2r^3(h-2r)f_{\mathcal{Q}}} \leq 0.$$

- $\tilde{\sigma} + \tilde{p}_r + 2\tilde{p}_\theta \geq 0 \Rightarrow \sigma + p_r + 2p_\theta \geq 0$, where

$$\begin{aligned} \frac{(2r-h)f_{\mathcal{Q}}}{r-h} &> 0 \text{ and } \frac{hr\left[\frac{2(hf_{\mathcal{Q}}\mathcal{Q}' + r^2(f_{\mathcal{T}}(p_r - P) + \kappa^2p_r))}{f} - \frac{hr^2}{h-2r}\right]}{\kappa^2r^6} \\ &+ \frac{\frac{h^2f_{\mathcal{Q}}(3h-rh'-2r)}{f(h-r)} + \frac{r^4(h-r)[2rf_{\mathcal{T}}(hP - (h-2r)p_\theta - Pr + \sigma r) - 2hf_{\mathcal{Q}}\mathcal{Q}' + fr(r-h) - 2\kappa^2r(hp_\theta + rp_r)]}{(h-2r)f_{\mathcal{Q}}}}{\kappa^2r^6} \geq 0. \end{aligned}$$

The above mentioned energy conditions are not satisfied in GR theory for traversable wormhole solutions. In particular, for positive energy density, the NEC must be violated as a consequence of the flaring-out condition at the wormhole throat. This requires presence of an exotic matter at the throat of the wormhole. Therefore, it is straightforward to extend this conclusion to modified gravity where the NEC must be violated effectively as verified by Eq. (19). However, the coupling between matter and geometry introduces additional degrees of freedom, which can mimic the effects of exotic matter or even replace it entirely keeping the physical matter healthy under specific conditions. This will be discussed in details in Sec. VI.

D. A particular $f(\mathcal{Q}, \mathcal{T})$ theory

To determine if traversable wormhole solutions are feasible, we will analyze the function $f(\mathcal{Q}, \mathcal{T})$ in the following way [43]:

$$f(\mathcal{Q}, \mathcal{T}) = \mathcal{Q} + \beta\mathcal{T}. \quad (34)$$

where β is a dimensional parameter with a dimension $[N^{-1}]$ similar to κ^2 . Therefore, in the following we use the transformation $\beta \rightarrow \beta\kappa^2$ where β is a dimensionless parameter. By utilizing the previously mentioned formula of $f(\mathcal{Q}, \mathcal{T})$, assuming a constant redshift function $\xi(r) = \xi_0$, in Eqs. (16)-(17), it yields

$$\sigma = \frac{(3 + 8\beta)h'}{3(1 + 2\beta)(1 + 4\beta)\kappa^2c^2r^2}, \quad (35)$$

$$p_r = -\frac{3(1 + 4\beta)h - 4\beta rh'}{3(1 + 2\beta)(1 + 4\beta)\kappa^2r^3}, \quad (36)$$

$$p_\theta = \frac{3(1 + 4\beta)h - (3 + 4\beta)rh'}{6(1 + 2\beta)(1 + 4\beta)\kappa^2r^3}. \quad (37)$$

For linear $f(\mathcal{Q}, \mathcal{T})$, we write the effective density and pressures in terms on the matter density ad pressures as follows:

$$\tilde{\sigma}c^2 = \sigma c^2 + \beta(3\sigma c^2 - p_r/3 - 2p_\theta/3), \quad (38)$$

$$\tilde{p}_r = p_r - \beta(\sigma c^2 - 7p_r/3 - 2p_\theta/3), \quad (39)$$

$$\tilde{p}_\theta = p_\theta - \beta(\sigma c^2 - p_r/3 - 8p_\theta/3). \quad (40)$$

Clearly the GR equations are recovered by setting $\beta = 0$. The above equations enable us to, alternatively, write the matter density and pressure in terms of the effective ones. These relations are important for determining the validity of the energy conditions within any modified gravity in principle. This will be discussed in details in Sec. VI.

IV. DARK MATTER DENSITY PROFILES

It has been shown that DM at the galactic halo could be consistent with wormholes structure [58, 59] as well as at the central region of the halo [60]. In the present study, we use Soliton+NFW DM density profiles to derive the corresponding shape functions, where soliton core model is applied at the central region of the DM halo and outer halo follows the NFW density profile which characterizes the CDM. This scenario is motivated by the famous core-cusp problem where N-body CDM simulations predict a cuspy density profile as $\sigma(r) \propto 1/r$ at small radii, while rotation curves of dwarf galaxies, where DM is dominating, point out a flat density profile at their cores. Another puzzle is known as the missing satellites problem, where CDM simulations predict more low-mass galaxies in the local group than the already observed. In this sense, the central masses are too low compared to the most massive (sub)halos predicted in Λ CDM.

Recent simulations of soliton+NFW DM scenario show that the galactic halos surround a dense core of dwarf spheroidal galaxies with a transition between the soliton core—characterized by a flat density profile—and the CDM halo at a radius of $\simeq 1.0$ kpc [61]; and also dwarf galaxies [62]. Therefore, the soliton+NFW model provides a good candidate to solve small radii problems related to Λ CDM scenario. We use the numerical values of the model parameters as obtained for the dwarf galaxy NGS 2366, using fuzzy DM (soliton+NFW) simulation, by the recent analysis [62], based on the rotation curves of the LITTLE THINGS in 3D catalog [63]. In the following, we are going to briefly discuss the two density profiles mentioned above.

A. Soliton quantum wave dark matter

Axions and other ultralight bosons, with masses $m_b \sim 10^{-23} - 10^{-21}$ eV, a well-known contender to address the aforementioned issues. At cosmological scales, these particles are consistent with the CDM. However, these particles behave as self-gravitating DM waves and populate the galactic halos with significant occupation numbers at distances comparable to their de Broglie wavelength, which can be in the kpc scale. The production of a flat core “soliton” at the center of galaxies with a rather marked transition to a less dense outer region that follows a CDM-like distribution is one of the repercussions of this, as it appears to have a pressure-like impact on macroscopic scales.

Assuming the simple case of ultralight bosons, when self-interaction is ignored, then the boson mass is the only free parameter. If the corresponding de Broglie wavelength exceeds the mean free path set by the density of dark matter, these bosons can satisfy the ground state condition for a Bose-Einstein condensate described by the coupled Schrödinger-Poisson equation. This can be written in comoving coordinates as

$$\left[i \frac{\partial}{\partial \tau} + \frac{1}{2} \nabla^2 - aV \right] \psi = 0, \\ \nabla^2 V = 4\pi(|\psi|^2 - 1),$$

where ψ is the wave function, V is the gravitation potential and a is the cosmological scale factor. The fitting formula for the density profile of the solitonic core in a ψ DM halo is obtained from cosmological simulations [64, 65]:

$$\sigma_{\text{sol}}(r) = \frac{\sigma_c}{\left[1 + \alpha (r/r_c)^2 \right]^8}, \quad (41)$$

here σ_c and r_c stand for the central density and size of the soliton core [66]. The leading study thoroughly examines the distribution of the matter that was previously mentioned [65]. The precise calculation for the half-density radius will be a specific radius that is determined as a constant $\alpha = \sqrt[8]{2} - 1 \sim 0.09051$ [64, 65]. Furthermore, the value of σ_c in Eq. (41) is specified as [66]:

$$\sigma_c = 2.4 \times 10^{12} \left(\frac{m_b}{10^{-22} \text{eV}} \right)^{-2} \left(\frac{r_c}{\text{pc}} \right)^{-4} \frac{M_\odot}{\text{pc}^3}. \quad (42)$$

We use the numerical values of the model parameters, r_c and ρ_c , using fuzzy DM simulation [62], based on the rotation curves of the LITTLE THINGS in 3D catalog [63]. For the dwarf galaxy NGC 2366, the core radius $r_c = 3$ kpc and the central density $\sigma_c = 15 \times 10^{-3} \text{ M}_\odot/\text{pc}^3$ [62].

B. Cold dark matter halo

We assume that the CDM distribution in the halo obeys NFW profile, which is extensively used in N -body simulation, therefore we write the NFW density profile [67]:

$$\sigma_{\text{NFW}}(r) = \frac{\sigma_s}{(r/r_s)(1+r/r_s)^2}. \quad (43)$$

In the above, r_s stands for the characteristic scale radius and σ_s is the corresponding scale density. The NFW halo density clearly goes as $\sigma_{\text{NFW}} \propto 1/r$ at small radii, while at large radii it goes as $\sigma_{\text{NFW}} \propto 1/r^3$. The characteristic scale density is related to the concentration parameter $c = r_{\text{vir}}/r_s$, with r_{vir} denotes the virial radius¹, and the cosmological matter density parameter $\Omega_m(z)$ as follows

$$\begin{aligned} \sigma_s &= \frac{\zeta(z)\sigma_{m0}}{3} \frac{c^3}{\log(1+c) - \frac{c}{1+c}}, \\ \zeta(z) &= \frac{18\pi^2 + 82(\Omega_m(z) - 1) - 39(\Omega_m(z) - 1)^2}{\Omega_m(z)}, \end{aligned}$$

where z denotes the redshift, and σ_{m0} is the current cosmological matter density, related to the critical density $\sigma_{c0} = 3H_0^2/8G$ with Hubble constant H_0 , by the following relation $\sigma_{m0} = \Omega_{m0}\sigma_{c0}$. Following the calculations as given in [62], we set $h = H_0/100 = 0.678$ and $\Omega_{m0} = 0.308$ as measured by Planck 2015. For the dwarf galaxy NGC 2366, we use a virial radius $r_{\text{vir}} = 5.5$ kpc as estimated for dwarf galaxies, where the concentration parameter for the NFW+baryons model is given by $c = 0.80^{+0.64}_{-0.35}$ [62], then we calculate the scale radius $r_s = 1.447$ kpc and the scale density $\sigma_s = 3.11 \times 10^{-3} \text{ M}_\odot/\text{pc}^3$.

V. EXAMINING DARK MATTER WORMHOLES

In this section, we utilize the dark matter density profiles discussed above, namely Eqs. (41) and (43), checking their viability to construct wormholes. This can be done by deriving the corresponding shape function, within linear $f(\mathcal{Q}, \mathcal{T})$ theory, by virtue of Eq. (35). Then, we examine possible constraints on the coupling strength between matter and geometry, β , in order to satisfy traversable wormhole conditions discussed in Sec. III A.

A. Model I

The exact shape function of a solitonic DM can be calculated by plugging the density profile (41) into Eq. (35):

$$h(r) = r_0 + A \left[\arctan(\sqrt{\alpha}r/r_c) - \arctan(\sqrt{\alpha}r_0/r_c) \right] + B \frac{r - r_0}{(r_c^2 + \alpha r^2)^7} \mathcal{F}(r). \quad (44)$$

The coefficients A and B are given as

$$\begin{aligned} A &= \frac{99\sigma_s c^2 \kappa^2 (1+2\beta)(1+4\beta)r_c^3}{2048\alpha\sqrt{\alpha}(3+8\beta)}, \\ B &= -\frac{99\sigma_s c^2 \kappa^2 (1+2\beta)(1+4\beta)r_c^4}{2048\alpha(3+8\beta)(r_c^2 + \alpha r_0^2)^7}, \end{aligned}$$

¹ The virial radius is defined as the radius where the average density falls to a critical threshold $\zeta(z)\sigma_{m0}$.

where $\beta \neq -3/8$ and the function $\mathcal{F}(r)$ is given by:

$$\begin{aligned}
\mathcal{F}(r) = & 680680r_c^8r_0^{11}r^7\alpha^9 + 680680r_c^8r_0^7r^{11}\alpha^9 + 3465r^{13}\alpha^{13}r_0^{13} + 3465r_c^{26} - 48580r_c^{24}\alpha r_0^2 - 48580r_c^{24}\alpha r^2 - 92323r_c^{22}\alpha^2r^4 \\
& - 92323r_c^{22}\alpha^2r_0^4 - 101376r_c^{20}\alpha^3r_0^6 - 101376r_c^{20}\alpha^3r^6 - 65373r_c^{18}\alpha^4r_0^8 - 23100r_c^{16}\alpha^5r_0^{10} - 3465r_c^{14}\alpha^6r_0^{12} - 65373r_c^{18}\alpha^4r^8 \\
& - 23100r_c^{16}\alpha^5r^{10} - 3465r_c^{14}\alpha^6r^{12} + 65373r_c^4r_0^9r^{13}\alpha^{11} + 23100r_c^2r_0^{13}r^{11}\alpha^{12} - 1155r_c^2r_0^{12}r^{12}\alpha^{12} + 23100r_c^2r_0^{11}r^{13}\alpha^{12} \\
& + 65373r_c^4r_0^{13}r^9\alpha^{11} - 7392r_c^4r_0^{12}r^{10}\alpha^{11} + 154308r_c^4r_0^{11}r^{11}\alpha^{11} - 7392r_c^4r_0^{10}r^{12}\alpha^{11} - 127820r_c^8r_0^{10}r^8\alpha^9 + 92323r_c^8r_0^5r^{13}\alpha^9 \\
& - 28952r_c^8r_0^6r^{12}\alpha^9 + 1245013r_c^8r_0^9r^9\alpha^9 + 101376r_c^6r_0^7r^{13}\alpha^{10} + 101376r_c^6r_0^{13}r^7\alpha^{10} - 19899r_c^6r_0^1r^{28}\alpha^{10} + 437712r_c^6r_0^{11}r^9\alpha^{10} \\
& - 47388r_c^6r_0^{10}r^{10}\alpha^{10} + 437712r_c^6r_0^9r^{11}\alpha^{10} - 19899r_c^6r_0^8r^{12}\alpha^{10} - 72835r_c^{24}\alpha r_0 - 165088r_c^{22}\alpha^2r_0r^3 - 165088r_c^{22}\alpha^2r_0^3r \\
& - 505148r_c^{22}\alpha^2r_0^2r^2 - 868912r_c^{20}\alpha^3r_0^4r^2 + 151268r_c^{20}\alpha^3r_0^3r^3 - 222651r_c^{20}\alpha^3r_0^5r - 222651r_c^{20}\alpha^3r_0r^5 - 868912r_c^{20}\alpha^3r_0^2r^4 \\
& - 1134763r_c^{18}\alpha^4r_0^4r^4 + 804020r_c^{18}\alpha^4r_0^5r^3 - 896280r_c^{18}\alpha^4r_0^2r^6 - 186648r_c^{18}\alpha^4r_0r^7 + 804020r_c^{18}\alpha^4r_0^3r^5 - 896280r_c^{18}\alpha^4r_0^6 \\
& - 186648r_c^{18}\alpha^4r_0^7r - 95865r_c^{16}\alpha^5r_0r^9 - 982072r_c^{16}\alpha^5r_0^6r^4 + 1146824r_c^{16}\alpha^5r_0^3r^7 - 982072r_c^{16}\alpha^5r_0^4r^6 - 553476r_c^{16}\alpha^5r_0^8r^2 \\
& - 95865r_c^{16}\alpha^5r_0^9r + 2249233r_c^{16}\alpha^5r_0^5r^5 - 553476r_c^{16}\alpha^5r_0^2r^8 + 1146824r_c^{16}\alpha^5r_0^7r^3 - 27720r_c^{14}\alpha^6r_0^{11}r - 542073r_c^{14}\alpha^6r_0^4r^8 \\
& + 2689232r_c^{14}\alpha^6r_0^5r^7 - 27720r_c^{14}\alpha^6r_0r^{11} + 2689232r_c^{14}\alpha^6r_0^7r^5 + 830760r_c^{14}\alpha^6r_0^9r^3 - 189420r_c^{14}\alpha^6r_0^2r^{10} - 542073r_c^{14}\alpha^6r_0^8r^4 \\
& + 830760r_c^{14}\alpha^6r_0^3r^9 - 858928r_c^{14}\alpha^6r_0^6r^6 - 189420r_c^{14}\alpha^6r_0^{10}r^2 + 1766023r_c^{12}r_0^5r^9\alpha^7 + 1942472r_c^{10}r_0^7r^9\alpha^8 - 28952r_c^{12}r_0^6r^6\alpha^9 \\
& + 92323r_c^{13}r_0^5\alpha^9 - 522032r_c^{12}r_0^6r^8\alpha^7 - 27720r_c^{12}r_0^2r^{12}\alpha^7 - 172760r_c^{12}r_0^{10}r^4\alpha^7 + 622076r_c^{10}r_0^{11}r^5\alpha^8 - 24185r_c^{10}r_0^4r^{12}\alpha^8 \\
& - 186424r_c^{10}r_0^6r^{10}\alpha^8 - 345583r_c^{10}r_0^8r^8\alpha^8 + 622076r_c^{10}r_0^5r^{11}\alpha^8 + 1942472r_c^{10}r_0^9r^7\alpha^8 + 48580r_c^{10}r_0^3r^{13}\alpha^8 + 48580r_c^{10}r_0^{13}r^3\alpha^8 \\
& - 186424r_c^{10}r_0^{10}r^6\alpha^8 - 24185r_c^{10}r_0^{12}r^4\alpha^8 - 3465r_c^{12}r_0r^{13}\alpha^7 + 312340r_c^{12}r_0^3r^{11}\alpha^7 + 3026128r_c^{12}r_0^7r^7\alpha^7 - 27720r_c^{12}r_0^2r^2\alpha^7 \\
& - 3465r_c^{12}r_0^{13}r\alpha^7 + 1766023r_c^{12}r_0^9r^5\alpha^7 + 312340r_c^{12}r_0^{11}r^3\alpha^7 - 522032r_c^{12}r_0^8r^6\alpha^7 - 172760r_c^{12}r_0^4r^{10}\alpha^7 - 127820r_c^8r_0^8r^{10}\alpha^9.
\end{aligned} \tag{45}$$

Obviously, at the wormhole throat, one obtains $h(r_0) = r_0$ as required by the throat condition of a traversable wormhole. Additionally, we apply the flaring-out condition at the the wormhole throat, $h'(r_0) < 1$, which gives

$$\frac{3\kappa^2\sigma_c c^2 r_0^2 r_c^{16} (1+2\beta)(1+4\beta)}{(3+8\beta)(r_c^2 + \alpha r_0^2)^8} < 1. \tag{46}$$

The above inequality sets the following constraints

$$\beta < -\frac{3}{8} + \frac{4(r_c^2 + \alpha r_0^2)^8 - \sqrt{16(r_c^2 + \alpha r_0^2)^{16} + 9\kappa^4\sigma_c^2 c^4 r_c^{32} r_0^4}}{24\kappa^2\sigma_c c^2 r_c^{16} r_0^2}, \text{ or} \tag{47}$$

$$-3/8 < \beta < -\frac{3}{8} + \frac{4(r_c^2 + \alpha r_0^2)^8 + \sqrt{16(r_c^2 + \alpha r_0^2)^{16} + 9\kappa^4\sigma_c^2 c^4 r_c^{32} r_0^4}}{24\kappa^2\sigma_c c^2 r_c^{16} r_0^2}. \tag{48}$$

The obtained intervals show the dependence of the parameter β on the wormhole size r_0 . For example, *assuming* $r_0 = 1$ pc, the flaring out condition is satisfied when $\beta < -3/8 - 8.494 \times 10^{-16}$ or $-3/8 < \beta < -3/8 + 1.840 \times 10^{13}$. However, for arbitrary values of $0 < r_0 < r_c$ one can set similar constraints on the non-minimal coupling parameter β satisfying $h'(r_0) < 1$. We show the parameter space $\{r_0, \delta\}$ graphically as seen in Fig. 1(a) by introducing the deviation factor, $\delta \equiv \beta + 3/8$, which measures the deviation from the restricted value $\beta = -3/8$. For $\delta > 0$, the non-minimal coupling parameter becomes large as $r_0 \rightarrow 0$ and smaller as $r \rightarrow r_c$. For $\delta < 0$ the deviation factor is tiny at $0 < r_0 < r_c$, where $\delta \sim -2 \times 10^{-9}$ as shown by the figure. We note that the excluded values in the parameter space $\{r_0, \delta\}$ must be considered when choosing the wormhole throat size r_0 to ensure its consistency with the flaring-out condition, see Fig. 1(b). The figure shows that the flaring-out condition at the throat, $(dh/dr)_{r_0} < 1$, is satisfied for different selected values of the parameter β .

In Fig. 2(a), for $r_0 = 1$ pc, we graphically show that the shape function (44) preserves the Lorentz signature, since $h(r)/r < 1$ at $r > r_0$ and it fulfills the asymptotic flatness condition $h(r)/r \rightarrow 0$ as $r \rightarrow \infty$. The figure shows also that the conditions related to the first derivative of the shape functions are fulfilled, i.e. $dh/dr < 1$ at $r > r_0$ and asymptotically $dh/dr \rightarrow 0$ as $r \rightarrow \infty$. Notably, the selected values of the parameter β are consistent with the outcome of the flaring-out condition at the wormhole throat (46).

For the static spherically symmetric spacetime solution we have just obtained, we take the time slice $t = \text{constant}$ on the equatorial plane $\theta = \pi/2$. Therefore the line element reads

$$ds^2 = \frac{dr^2}{1 - h(r)/r} + r^2 d\Phi^2. \tag{49}$$

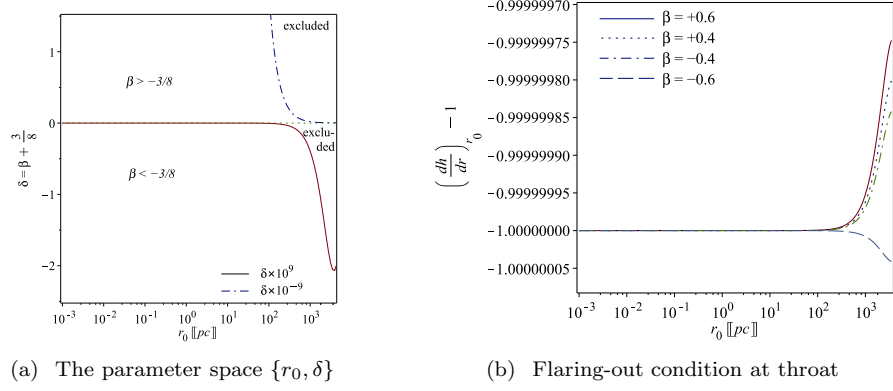


FIG. 1. Model I: (a) The parameter space $\{r_0, \delta\}$ of the soliton DM core wormhole model of galaxy NGC 2366 ($\sigma_c = 15 \times 10^{-3} M_\odot/\text{pc}^3$ and $r_c = 3$ kpc [62]). We use the faring out constraint on the shape function at the wormhole throat $h'(r_0) < 1$ to evaluate critical values of the non-minimal coupling parameter β , namely (47) and (48), at arbitrary throat size $0 < r_0 < r_c$ where r_c is the soliton core radius of galaxy NGC 2366. Given that $\beta \neq -3/8$, we show both cases when $\beta < -3/8$ ($\delta < 0$) and $\beta > -3/8$ ($\delta > 0$). The positive (negative) δ curve is multiplied by a factor 10^{-9} (10^9) to fit the curve into the scale of the graph. (b) The flaring-out condition at the wormhole throat is satisfied for different selected values of the parameter β where the wormhole throat is arbitrarily chosen $0 < r_0 < r_c$, it shows that $h'(r_0) < 1$ is fulfilled.

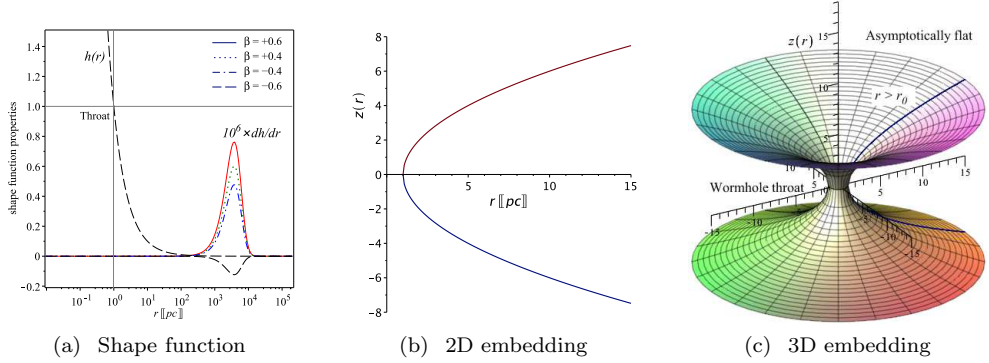


FIG. 2. Model I: wormhole embedding diagrams: (a) The plots show that $h(r) < r$ and $h'(r) < 1$ at $r > r_0$, while $h/r \rightarrow 0$ and $h' \rightarrow 0$ as $r \rightarrow \infty$. (b) The embedding surface integral, Eq. (51), shows that $z'(r_0) \rightarrow \infty$, $z(r > r_0)$ is finite and $z(r) \rightarrow \infty$ as $r \rightarrow \infty$. (c) Since $z'(r_0) \rightarrow \infty$, then $z(r)$ is vertical in the 3D embedding diagram. We set $r_0 = 1$ pc, for the galaxy NGC 2366, where $\sigma_c = 15 \times 10^{-3} M_\odot/\text{pc}^3$ and $r_c = 3$ kpc [62].

To visualize the wormhole, we embed the above surface in R^3 Euclidean space cylindrical coordinate (r, Φ, z)

$$ds^2 = \left[1 + \left(\frac{dz}{dr} \right)^2 \right] dr^2 + r^2 d\Phi^2. \quad (50)$$

Thus, the embedding surface integral is given as

$$z(r) = \pm \int_{r_0}^r \frac{d\zeta}{\sqrt{\zeta/h(\zeta) - 1}}. \quad (51)$$

In Fig. 2(b), we represent the embedding surface integral (2D embedding) diagram (51) corresponds to the soliton shape function (44). It can be noted that at the wormhole throat

$$\lim_{r \rightarrow r_0} dz/dr \rightarrow \infty,$$

therefore $z(r)$ is vertical in the 3D embedding diagram in Fig. 2(c).

B. Model II

The exact shape function of CDM can be calculated by plugging the NFW density profile (43), into Eq. (35):

$$h(r) = r_0 + \tilde{A} \frac{r - r_0}{r + r_s} + \tilde{B} \ln \left[\frac{r + r_s}{r_0 + r_s} \right], \quad (52)$$

where the coefficients \tilde{A} and \tilde{B} are given as

$$\begin{aligned} \tilde{A} &= -\frac{3\sigma_s c^2 \kappa^2 (1+2\beta)(1+4\beta)r_s^4}{(3+8\beta)(r_0+r_s)}, \\ \tilde{B} &= -\tilde{A} \left(1 + \frac{r_0}{r_s}\right) = \frac{3\sigma_s c^2 \kappa^2 (1+2\beta)(1+4\beta)r_s^3}{(3+8\beta)}. \end{aligned}$$

Obviously, at the wormhole throat, one obtains $h(r_0) = r_0$ as required by the throat condition of a traversable wormhole. Additionally, we apply the flaring-out condition at the the wormhole throat, $h'(r_0) < 1$, which gives

$$\frac{3\kappa^2 \sigma_s c^2 r_0 r_s^3 (1+2\beta)(1+4\beta)}{(3+8\beta)(r_s+r_0)^2} < 1. \quad (53)$$

The above inequality sets the following constraints

$$\beta < -\frac{3}{8} + \frac{4(r_s + r_0)^2 - \sqrt{16(r_s + r_0)^4 + 9\kappa^4 \sigma_s^2 c^4 r_s^6 r_0^2}}{24\kappa^2 \sigma_s c^2 r_s^3 r_0}, \text{ or} \quad (54)$$

$$-3/8 < \beta < -\frac{3}{8} + \frac{4(r_s + r_0)^2 + \sqrt{16(r_s + r_0)^4 + 9\kappa^4 \sigma_s^2 c^4 r_s^6 r_0^2}}{24\kappa^2 \sigma_s c^2 r_s^3 r_0}. \quad (55)$$

The obtained intervals show the dependence of the parameter β on the wormhole size r_0 . For example, *assuming* $r_0 = 1$ kpc, the flaring out condition is satisfied when $\beta < -3/8 - 2.545 \times 10^{-13}$ or $-3/8 < \beta < -3/8 + 6.140 \times 10^{10}$. However, for arbitrary values of $0 < r_0 < r_c$ one can set similar constraints on the non-minimal coupling parameter β satisfying $h'(r_0) < 1$. We show the parameter space $\{r_0, \delta\}$ graphically as seen in Fig. 3(a) by introducing the deviation factor, $\delta \equiv \beta + 3/8$, which measures the deviation from the restricted value $\beta = -3/8$. For $\delta > 0$, the non-minimal coupling parameter becomes large as $r_0 \rightarrow 0$ and smaller as $r \rightarrow r_s$. For $\delta < 0$ the deviation factor is tiny at $0 < r_0 < r_s$, where $\delta \sim -1 \times 10^{-10}$ as shown by the figure. We note that the excluded values in the parameter space $\{r_0, \delta\}$ must be considered when choosing the wormhole throat size r_0 to ensure its consistency with the flaring-out condition, see Fig. 3(b). The figure shows that the flaring-out condition at the throat, $(dh/dr)_{r_0} < 1$, is satisfied for different selected values of the parameter β .

In Fig. 4(a), for $r_0 = 1$ kpc, we graphically show that the shape function (52) preserves the Lorentz signature, since $h(r)/r < 1$ at $r > r_0$ and it fulfills the asymptotic flatness condition $h(r)/r \rightarrow 0$ as $r \rightarrow \infty$. The figure shows also that the conditions related to the first derivative of the shape functions are fulfilled, i.e. $dh/dr < 1$ at $r > r_0$ and asymptotically $dh/dr \rightarrow 0$ as $r \rightarrow \infty$. Notably, the selected values of the parameter β are consistent with the outcome of the flaring-out condition at the wormhole throat (53).

Similar to Sec. V A, we visualize the wormhole solution (52), where the corresponding embedding surface integral (51) is as seen in Fig. 4(b). We note that at the wormhole throat

$$\lim_{r \rightarrow r_0} dz/dr \rightarrow \infty,$$

therefore $z(r)$ is vertical in the 3D embedding diagram in Fig. 4(c).

In summary, we have shown that two DM models are consistent with the wormhole structure in presence of non-minimal coupling between matter and geometry. The first model assumes soliton quantum wave DM at the galactic core, where the density profile follows Eq. (41) and the corresponding wormhole shape function is obtained by Eq. (44). The second assumes CDM presence at the galactic halo, where the density profile follows the NFW ansatz (43) and the corresponding wormhole shape function is obtained by Eq. (52). We investigated possible constraints on the non-minimal coupling parameter β from the wormhole flaring-out condition. For the dwarf galaxy NGC 2366, recalling the values of the parameters of the soliton+NFW DM model as studied in [62], we found the following constraints: In model I, we obtained the viable parameter space $\{\beta, r_0\}$ as given by (47) and (48), and by setting $r_0 = 1$ pc, these give $\beta < -3/8 - 8.494 \times 10^{-16}$ or $-3/8 < \beta < 1.840 \times 10^{13}$. In model II, we obtained the viable parameter space $\{\beta, r_0\}$ as given by (54) and (55), and by setting $r_0 = 1$ pc, these give $\beta < -3/8 - 2.545 \times 10^{-13}$ or $-3/8 < \beta < 6.140 \times 10^{10}$. In general, for the corresponding valid regions of the coupling parameter β , the wormhole models fulfill the following constraints:

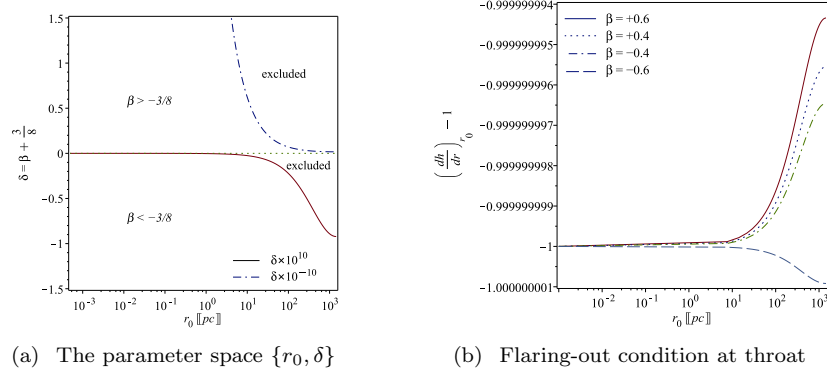


FIG. 3. Model II: (a) The parameter space $\{r_0, \delta\}$ of the NFW CDM wormhole model of galaxy NGC 2366 ($\sigma_s = 3.11 \times 10^{-3} M_\odot/\text{pc}^3$ and $r_s = 1.447 \text{ kpc}$). We use the faring out constraint on the shape function at the wormhole throat $h'(r_0) < 1$ to evaluate critical values of the non-minimal coupling parameter β , namely (54) and (55), at arbitrary throat size $0 < r_0 < r_c$ where r_c is the soliton core radius of galaxy NGC 2366. Given that $\beta \neq -3/8$, we show both cases when $\beta < -3/8$ ($\delta < 0$) and $\beta > -3/8$ ($\delta > 0$). The positive (negative) δ curve is multiplied by a factor 10^{-10} (10^{10}) to fit the curve into the scale of the graph. (b) The flaring-out condition at the wormhole throat is satisfied for different selected values of the parameter β where the wormhole throat is arbitrarily chosen $0 < r_0 < r_s$, it shows that $h'(r_0) < 1$ is fulfilled.

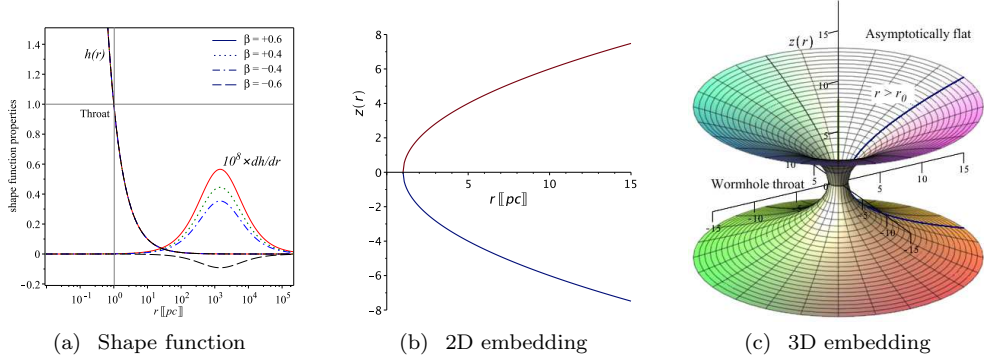


FIG. 4. Model II: wormhole embedding diagrams: (a) The plots show that $h(r) < r$ and $h'(r) < 1$ at $r > r_0$, while $h/r \rightarrow 0$ and $h' \rightarrow 0$ as $r \rightarrow \infty$. (b) The embedding surface integral, Eq. (51), shows that $z'(r_0) \rightarrow \infty$, $z(r > r_0)$ is finite and $z(r) \rightarrow \infty$ as $r \rightarrow \infty$. (c) Since $z'(r_0) \rightarrow \infty$, then $z(r)$ is vertical in the 3D embedding diagram. We set $r_0 = 1 \text{ pc}$, for the galaxy NGC 2366, $\sigma_s = 3.11 \times 10^{-3} M_\odot/\text{pc}^3$ and $r_s = 1.447 \text{ kpc}$ [62].

- (i) At the throat $r = r_0$; the shape function $h(r_0) = r_0$, $h'(r_0) < 1$, $z(r_0) = 0$ and $z'(r_0) \rightarrow \infty$.
- (ii) At finite radius $r > r_0$; the shape function $h(r) < r$, $h'(r) < 1$, $z(r)$ is finite and $z'(r)$ is finite.
- (iii) At infinite distance from the wormhole $r \rightarrow \infty$; the shape function satisfies $h(r)/r \rightarrow 0$, $h'(r) \rightarrow 0$, $z(r) \rightarrow \pm\infty$ and $z'(r) \rightarrow 0$.

VI. ENERGY CONDITIONS OF DARK MATTER WORMHOLES IN $f(\mathcal{Q}, \mathcal{T})$ GRAVITY

In the context of GR, the focusing theorem implies the positivity of the tidal tensor trace $\mathfrak{R}_{\alpha\beta}u^\alpha u^\beta \geq 0$ and $\mathfrak{R}_{\alpha\beta}\ell^\alpha\ell^\beta \geq 0$ in Raychaudhuri equation, where u^α is an arbitrary timelike vector and ℓ^α is an arbitrary future directed null vector. This imposes four conditions on the energy-momentum tensor $\mathfrak{T}^{\alpha\beta}$, those are the energy conditions. These could be extended to modified gravity. In the particular case of $f(\mathcal{Q}, \mathcal{T})$ gravity the energy conditions could be written in terms of the effective energy-momentum tensor $\tilde{\mathfrak{T}}^\alpha_\beta = \text{diag}(-\tilde{\rho}c^2, \tilde{p}_r, \tilde{p}_t, \tilde{p}_\theta)$, since $\mathfrak{R}_{\alpha\beta} = \kappa \left(\tilde{\mathfrak{T}}_{\alpha\beta} - \frac{1}{2}g_{\alpha\beta}\tilde{\mathfrak{T}} \right)$. A physical model should satisfy the modified energy conditions as stated below:

- a. Weak energy condition (WEC): $\tilde{\sigma} \geq 0$, $\tilde{\sigma}c^2 + \tilde{p}_r > 0$, $\tilde{\sigma}c^2 + \tilde{p}_\theta > 0$,

- b. Null energy condition (NEC): $\tilde{\sigma}c^2 + \tilde{p}_r \geq 0$, $\tilde{\sigma}c^2 + \tilde{p}_\theta \geq 0$,
- c. Strong energy condition (SEC): $\tilde{\sigma}c^2 + \tilde{p}_r + 2\tilde{p}_\theta \geq 0$, $\tilde{\sigma}c^2 + \tilde{p}_r \geq 0$, $\tilde{\sigma}c^2 + \tilde{p}_\theta \geq 0$,
- d. Dominant energy conditions (DEC): $\tilde{\sigma} \geq 0$, $\tilde{\sigma}c^2 - \tilde{p}_r \geq 0$ and $\tilde{\sigma}c^2 - \tilde{p}_\theta \geq 0$.

For linear $f(\mathcal{Q}, \mathcal{T})$, we have obtained the effective density and pressures, namely Eqs. (38)–(40), which allow us to write the corresponding energy conditions as follows:

$$\tilde{\sigma}c^2 + \tilde{p}_r = (1 + 2\beta)(\sigma c^2 + p_r), \quad (56)$$

$$\tilde{\sigma}c^2 + \tilde{p}_\theta = (1 + 2\beta)(\sigma c^2 + p_\theta), \quad (57)$$

$$\tilde{\sigma}c^2 - \tilde{p}_r = \sigma dc^2 - p_r + 4\beta(\sigma c^2 - p_r/3 - 2p_\theta/3), \quad (58)$$

$$\tilde{\sigma}c^2 - \tilde{p}_r = \sigma c^2 - p_\theta + 2\beta(2\sigma c^2 - p_r/3 - 5p_\theta/3), \quad (59)$$

$$\tilde{\sigma}c^2 + \tilde{p}_r + \tilde{p}_\theta = \sigma c^2 + p_r + 2p_\theta + \frac{8}{3}\beta(p_r + 2p_\theta). \quad (60)$$

It has been noted that the flaring-out condition of a traversable wormhole—in the GR context—is necessarily inconsistent with the NEC [68], if the energy density is positive. Interestingly, the above relations show that the flaring-out condition can be reconciled with the NEC in the context of $f(\mathcal{Q}, \mathcal{T})$ modified gravity. According to Eqs. (20) and (21), one must have $\tilde{\sigma}c^2 + \tilde{p}_r < 0$ when the flaring-out condition holds. However, for the matter sector, one could have $\sigma c^2 + p_r > 0$ and $\beta < -1/2$, and therefore the NEC is fulfilled. Similar argument can be applied for condition (57). In this case, the NEC condition is broken only effectively, whereas the matter sector preserves the NEC with no need to exotic matter. We remark that $\beta < -1/2$ is consistent with our findings by applying the flaring-out condition in the previous section. In the following we test the energy conditions of the obtained wormhole models.

A. Model I

Plugging the soliton shape function (44) into Eqs. (36) and (37), we obtain

$$\begin{aligned} p_r = & -\frac{A \left[\arctan \left(\frac{\sqrt{\alpha}r}{r_c} \right) - \arctan \left(\frac{\sqrt{\alpha}r_0}{r_c} \right) \right]}{\kappa^2 r^3 (1 + 2\beta)} + \frac{1}{3(r_c^2 + \alpha r^2)^8 \kappa^2 (1 + 2\beta) (8\beta + 1) r^3} [136\beta r^2 \mathcal{F}(r) \alpha r_0 + 8\beta r^2 \mathcal{F}'(r) r_c^2 \\ & + 8\beta r^4 \mathcal{F}'(r) \alpha - 16\beta r \mathcal{F}(r) r_c^2 - 128\beta r^3 \mathcal{F}(r) \alpha + 3\mathcal{F}(r) r_0 \alpha r^2 + 24\beta \mathcal{F}(r) r_0 r_c^2 + 56\beta r^3 A \alpha^{\frac{3}{2}} r_c^{13} + 168\beta r^5 A \alpha^{\frac{5}{2}} r_c^{11} \\ & + 280\beta r^7 A \alpha^{\frac{7}{2}} r_c^9 + 280\beta r^9 A \alpha^{\frac{9}{2}} r_c^7 + 168\beta r^{11} A \alpha^{\frac{11}{2}} r_c^5 + 56\beta r^{13} A \alpha^{\frac{13}{2}} r_c^3 + 8\beta r^{15} A \alpha^{\frac{15}{2}} r_c - 192\beta r_0 r_c^{14} \alpha r^2 - 672\beta r_0 r_c^{12} \alpha^2 r^4 \\ & - 1344\beta r_0 r_c^{10} \alpha^3 r^6 - 1680\beta r_0 r_c^8 \alpha^4 r^8 - 1344\beta r_0 r_c^6 \alpha^5 r^{10} - 672\beta r_0 r_c^4 \alpha^6 r^{12} - 192\beta r_0 r_c^2 \alpha^7 r^{14} + 8\beta r A \sqrt{\alpha} r_c^{15} \\ & - 8\beta r \mathcal{F}'(r) r_0 r_c^2 - 8\beta r^3 \mathcal{F}'(r) r_0 \alpha - 24r_0 r_c^{14} \alpha r^2 - 84r_0 r_c^{12} \alpha^2 r^4 - 168r_0 r_c^{10} \alpha^3 r^6 - 210r_0 r_c^8 \alpha^4 r^8 - 168r_0 r_c^6 \alpha^5 r^{10} \\ & - 84r_0 r_c^4 \alpha^6 r^{12} - 24r_0 r_c^2 \alpha^7 r^{14} - 24\beta r_0 \alpha^8 r^{16} - 3\mathcal{F}(r) r r_c^2 - 3\mathcal{F}(r) r^3 \alpha + 3\mathcal{F}(r) r_0 r_c^2 - 3r_0 r_c^{16} - 3r_0 \alpha^8 r^{16} - 24\beta r_0 r_c^{16}] , \end{aligned} \quad (61)$$

$$\begin{aligned} p_\theta = & \frac{A \left[\arctan \left(\frac{\sqrt{\alpha}r}{r_c} \right) - \arctan \left(\frac{\sqrt{\alpha}r_0}{r_c} \right) \right]}{2\kappa^2 r^3 (1 + 2\beta)} + \frac{1}{6(r_c^2 + \alpha r^2)^8 \kappa^2 r^3 (1 + 10\beta + 16\beta^2)} [-(8\beta + 3) r_c A r^{15} \alpha^{15/2} \\ & - 21(8\beta + 3) r_c^5 A r^{11} \alpha^{\frac{11}{2}} - 7(8\beta + 3) r_c^3 A r^{13} \alpha^{\frac{13}{2}} - 35(8\beta + 3) r_c^7 A r^9 \alpha^{9/2} - 7(8\beta + 3) r_c^{13} A r^3 \alpha^{3/2} - 21(8\beta + 3) r_c^{11} A r^5 \alpha^{5/2} \\ & - 35(8\beta + 3) r_c^9 A r^7 \alpha^{7/2} + 3r_0 (8\beta + 1) (r_c^2 + \alpha r^2)^8 - (8\beta + 3) (r - r_0) r (r_c^2 + \alpha r^2) \mathcal{F}'(r) - (8\beta + 3) r_c^{15} A r \sqrt{\alpha} \\ & + ((128\beta + 42) \alpha r^3 - r_0 (45 + 136\beta) \alpha r^2 + 16\beta r r_c^2 - 3r_0 r_c^2 (8\beta + 1)) \mathcal{F}(r)] . \end{aligned} \quad (62)$$

We select $\beta = -0.6$ which is consistent with the flaring-out condition and the NEC $\sigma c^2 + p_r > 0$ (i.e. $\beta < -1/2$). We plot the density profile of the soliton core model of galaxy NGC 2366, the radial and the tangential pressures as shown in Fig. 5(a). The figure shows the flat density profile as suggested to solve the core-cusp problem, while

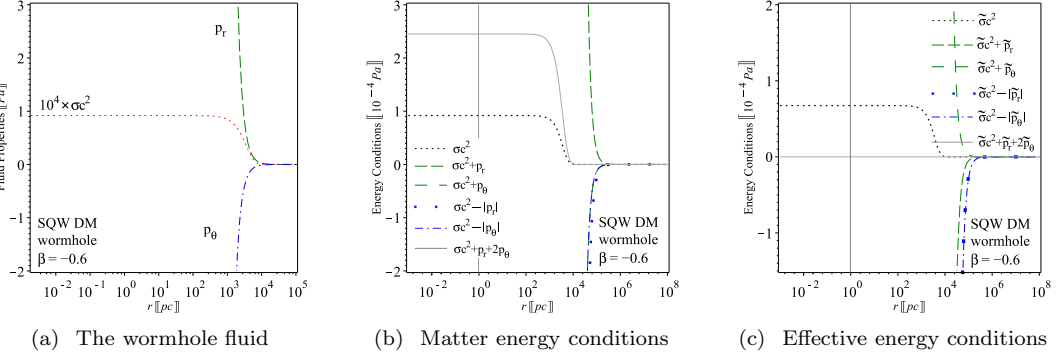


FIG. 5. Model I with $\beta = -0.6$: (a) The wormhole fluid, the density has a flat profile at the core as suggested to solve the core-cusp problem with $p_r > 0$ and $p_\theta < 0$. (b) The matter energy conditions, where the NEC $\sigma c^2 + p_r > 0$ is satisfied and $\sigma c^2 + p_\theta < 0$ at $r > r_0$. (c) The effective energy conditions, where the NEC $\tilde{\sigma} c^2 + \tilde{p}_r > 0$ is broken, but $\tilde{\sigma} c^2 + \tilde{p}_\theta > 0$ is satisfied at $r > r_0$. The alternative behavior of the NEC in the matter and the effective sector is understood since $\beta = -0.6 < -1/2$, see Eqs. (56) and (57). Other energy conditions, namely SEC and DEC, are broken in both sectors. We set $r_0 = 1$ pc, for the galaxy NGC 2366, where $\sigma_c = 15 \times 10^{-3} M_\odot/\text{pc}^3$ and $r_c = 3$ kpc [62].

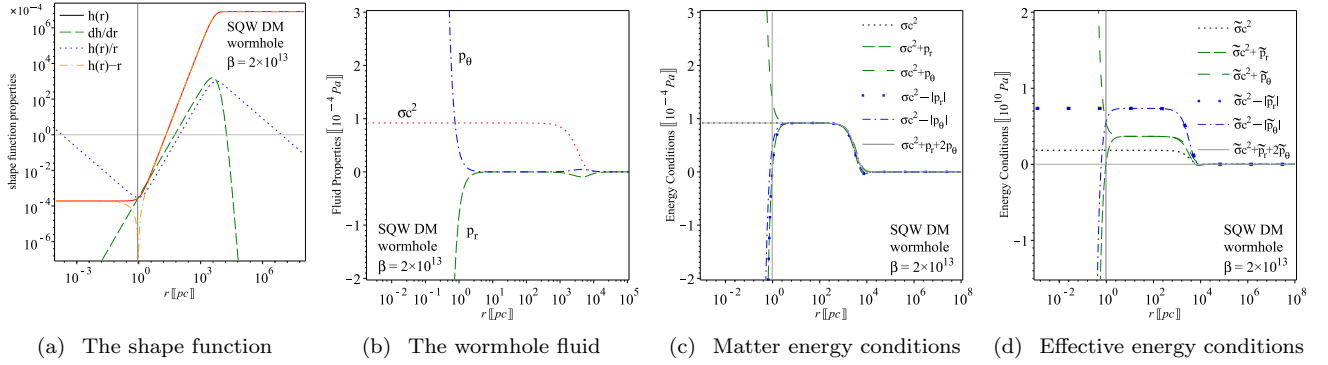


FIG. 6. Model I with large positive coupling $\beta \geq 1.840 \times 10^{13}$: (a) The wormhole is not Lorentzian as $h(r) > r$ at $r > r_0$, additionally the flaring-out condition is broken. (b) The matter fluid, the density has a flat profile at the core as suggested to solve the core-cusp problem with $p_r < 0$ and $p_\theta > 0$. (c) The matter energy conditions are fulfilled at $r > r_0$. (d) The effective energy conditions are fulfilled at $r > r_0$. We set $r_0 = 1$ pc, for the galaxy NGC 2366, where $\sigma_c = 15 \times 10^{-3} M_\odot/\text{pc}^3$ and $r_c = 3$ kpc [62].

$p_r > 0$ and $p_\theta < 0$ for $r > r_0$ where $r_0 = 1$ pc. The corresponding energy conditions on the matter fluid are presented in Fig. 5(b), which clearly show that the NEC $\sigma c^2 + p_r > 0$ is fulfilled at $r > r_0$. Since $\beta < -1/2$, the NEC is broken effectively as $\tilde{\sigma} c^2 + \tilde{p}_r < 0$ as shown in Fig. 5(c). On the other hand, one can find that $\sigma c^2 + p_\theta < 0$, where $\tilde{\sigma} c^2 + \tilde{p}_\theta > 0$. Other energy constraints on the matter and the effective sectors are also shown in Figs. 5(b) and 5(c).

Substituting (41), (61) and (62) into the energy conditions, one can accordingly set some constraints on the non-minimal coupling parameter β . By solving the energy conditions on the matter sector, we find the following constraints $\beta \leq -5.519 \times 10^{13}$ or $\beta \geq 1.840 \times 10^{13}$. Remarkably, for the same r_0 , we have shown that the faring-out condition gives $\beta < -3/8 - 8.494 \times 10^{-16}$ or $-3/8 < \beta < 1.840 \times 10^{13}$. Therefore, the flaring-out condition excludes the interval $\beta \geq 1.840 \times 10^{13}$. In the following we discuss both cases in more detail.

For large positive $\beta \geq 1.840 \times 10^{13}$, the matter density and pressures are given in Fig. 6(b). It can be noted that all energy conditions are satisfied for both the matter and the effective (including the non-minimal coupling effect) sectors at $r > r_0$ as seen in Figs. 6(c) and 6(d). However, the flaring-out condition and the Lorentzian signature conditions are clearly broken as shown in Fig. 6(a). This confirms the exclusion the interval $\beta \geq 1.840 \times 10^{13}$ as it cannot represent a traversable wormhole.

For large negative $\beta \leq -5.519 \times 10^{13}$, the matter density and pressures are given in Fig. 7(b). It can be noted that all energy conditions are satisfied for the matter fluid at $r > r_0$ as seen in Figs. 7(c). On the contrary, the energy conditions are broken on the effective sector as seen by Fig. 7(d), which is must occur if the flaring-out of the wormhole is hold. In Fig. 7(a), we show that the wormhole solution, in this case, satisfies all conditions related to the shape function and its derivative.

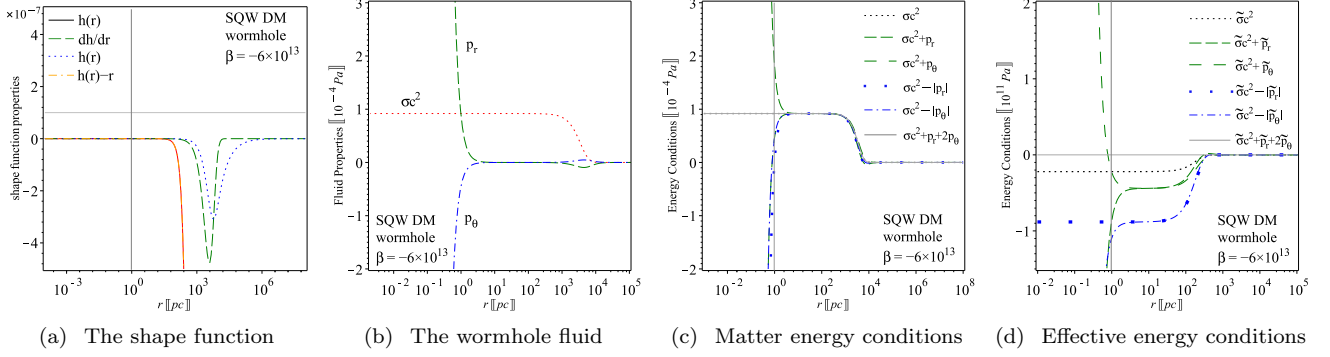


FIG. 7. Model I with large negative coupling $\beta \leq -5.519 \times 10^{13}$: (a) The wormhole is Lorentzian as $h(r) < r$ at $r > r_0$, additionally the flaring-out condition is fulfilled. (b) The matter fluid, the density has a flat profile at the core as suggested to solve the core-cusp problem with $p_r > 0$ and $p_\theta < 0$. (c) The matter energy conditions are fulfilled at $r > r_0$. (d) The effective energy conditions are broken at $r > r_0$ which represents the GR case. We set $r_0 = 1$ pc, for the galaxy NGC 2366, where $\sigma_c = 15 \times 10^{-3} M_\odot/\text{pc}^3$ and $r_c = 3$ kpc [62].

In conclusion, the above calculations confirm the possibility to find a healthy wormhole solution where the energy conditions are broken only on the effective sector but satisfied on the matter sector. Consequently, no exotic matter is needed to form a physical wormhole as required in the GR framework, if non-minimal coupling between matter and geometry has been considered and stays within certain bounds.

B. Model II

Substituting the NFW shape function (52) into Eqs. (36) and (37), we obtain

$$p_r = -\frac{\left[r_0 + \tilde{A}\frac{(r-r_0)}{(r+r_s)} + \tilde{B}\ln\left(\frac{r_s+r}{r_s+r_0}\right)\right]}{(1+2\beta)\kappa^2 r^3} + \frac{4\beta\left[(\tilde{A}+\tilde{B})r_s + \tilde{A}r_0 + \tilde{B}r\right]}{3(r_s+r)^2(1+2\beta)(1+4\beta)\kappa^2 r^2}, \quad (63)$$

$$p_\theta = \frac{\left[r_0 + \tilde{A}\frac{(r-r_0)}{(r+r_s)} + \tilde{B}\ln\left(\frac{r_s+r}{r_s+r_0}\right)\right]}{2(1+2\beta)\kappa^2 r^3} + \frac{(3+4\beta)\left[(\tilde{A}+\tilde{B})r_s + \tilde{A}r_0 + \tilde{B}r\right]}{6(r_s+r)^2(1+2\beta)(1+4\beta)\kappa^2 r^2}. \quad (64)$$

We select $\beta = -0.6$ which is consistent with the flaring-out condition and the NEC $\sigma c^2 + p_r > 0$ (i.e. $\beta < -1/2$). We plot the density profile of the CDM model of galaxy NGC 2366, the radial and the tangential pressures as shown in Fig. 8(a). The figure shows the cuspy behavior of the density profile at the core region, while $p_r > 0$ and $p_\theta < 0$ for $r > r_0$ where $r_0 = 1$ pc. The corresponding energy conditions on the matter fluid are presented in Fig. 8(b), which clearly show that the NEC $\sigma c^2 + p_r > 0$ is fulfilled at $r > r_0$. Since $\beta < -1/2$, the NEC is broken effectively as $\tilde{\sigma} c^2 + \tilde{p}_r < 0$ as shown in Fig. 8(c). On the other hand, one can find that $\sigma c^2 + p_\theta < 0$, where $\tilde{\sigma} c^2 + \tilde{p}_\theta > 0$. Other energy constraints on the matter and the effective sectors are also shown in Figs. 8(b) and 8(c).

Substituting (43), (63) and (64) into the energy conditions, one can accordingly set some constraints on the non-minimal coupling parameter β . By solving the energy conditions on the matter sector, we find the following constraints $\beta \leq -1.842 \times 10^{11}$ or $\beta \geq 6.140 \times 10^{10}$. Remarkably, for the same r_0 , we have shown that the flaring-out condition gives $\beta < -3/8 - 2.545 \times 10^{-13}$ or $-3/8 < \beta < 6.140 \times 10^{10}$. Therefore, the flaring-out condition excludes the interval $\beta \geq 6.140 \times 10^{10}$. In the following we discuss both cases in more detail.

For large positive $\beta \geq 6.140 \times 10^{10}$, the matter density and pressures are given in Fig. 9(b). It can be noted that all energy conditions are satisfied for both the matter and the effective (including the non-minimal coupling effect) sectors at $r > r_0$ as seen in Figs. 9(c) and 9(d). However, the flaring-out condition and the Lorentzian signature conditions are clearly broken as shown in Fig. 9(a). This confirms the exclusion the interval $\beta \geq 5.388 \times 10^6$ as it cannot represent a traversable wormhole.

For large negative $\beta \leq -1.842 \times 10^{11}$, the matter density and pressures are given in Fig. 10(b). It can be noted that all energy conditions are satisfied for the matter fluid at $r > r_0$ as seen in Figs. 10(c). On the contrary, the energy conditions are broken on the effective sector as seen by Fig. 10(d), which is must occur if the flaring-out of the wormhole is hold. In Fig. 10(a), we show that the wormhole solution, in this case, satisfies all conditions related to the shape function and its derivative.

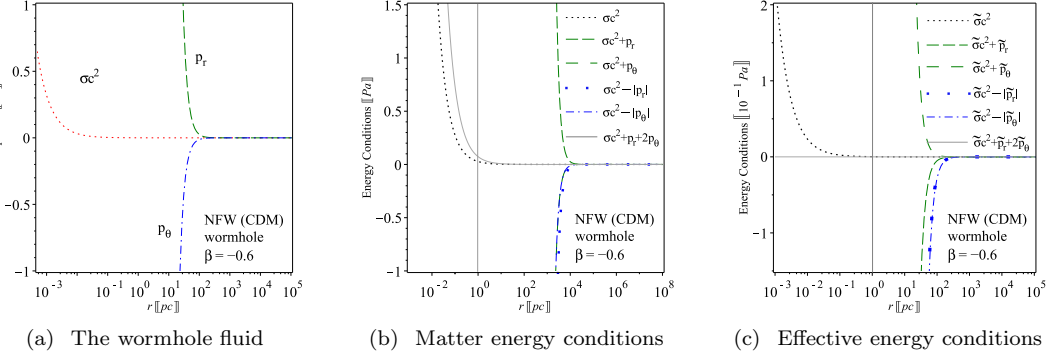


FIG. 8. Model II with $\beta = -0.6$: (a) The matter fluid, the density has a flat profile at the core as suggested to solve the core-cusp problem with $p_r > 0$ and $p_\theta < 0$. (b) The matter energy conditions, where the NEC $\sigma c^2 + p_r > 0$ is satisfied and $\sigma c^2 + p_\theta < 0$ at $r > r_0$. (c) The effective energy conditions, where the NEC $\tilde{\sigma} c^2 + \tilde{p}_r > 0$ is broken, but $\tilde{\sigma} c^2 + \tilde{p}_\theta > 0$ is satisfied at $r > r_0$. The alternative behavior of the NEC in the matter and the effective sector is understood since $\beta = -0.6 < -1/2$, see Eqs. (56) and (57). Other energy conditions, namely SEC and DEC, are broken in both sectors. We set $r_0 = 1$ pc, for the galaxy NGC 2366, $\sigma_s = 3.11 \times 10^{-3} \text{ M}_\odot/\text{pc}^3$ and $r_s = 1.447$ kpc [62].

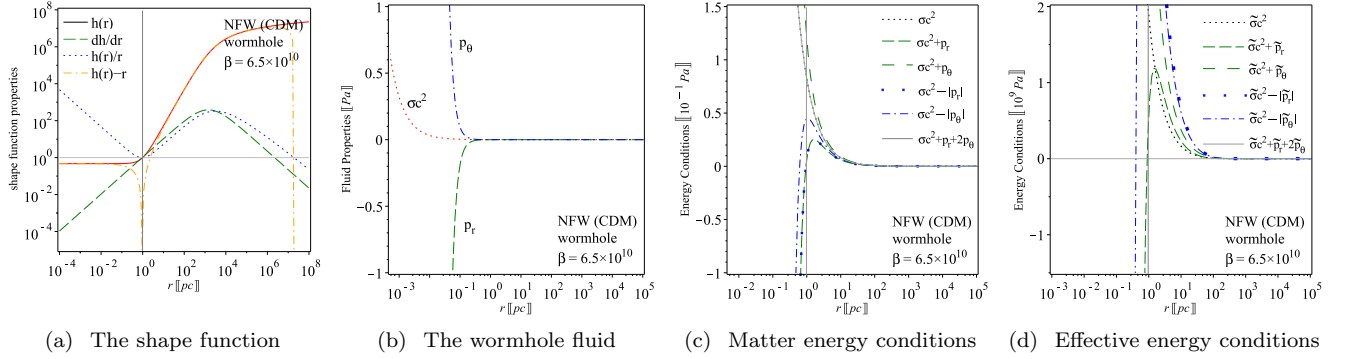


FIG. 9. Model II with large positive coupling $\beta \geq 6.140 \times 10^{10}$: (a) The wormhole is not Lorentzian as $h(r) > r$ at $r > r_0$, additionally the flaring-out condition is broken. (b) The matter fluid, the density has a cuspy profile at the core region, whereas $p_r < 0$ and $p_\theta > 0$. (c) The matter energy conditions are fulfilled at $r > r_0$. (d) The effective energy conditions are fulfilled at $r > r_0$. We set $r_0 = 1$ pc, for the galaxy NGC 2366, $\sigma_s = 3.11 \times 10^{-3} \text{ M}_\odot/\text{pc}^3$ and $r_s = 1.447$ kpc [62].

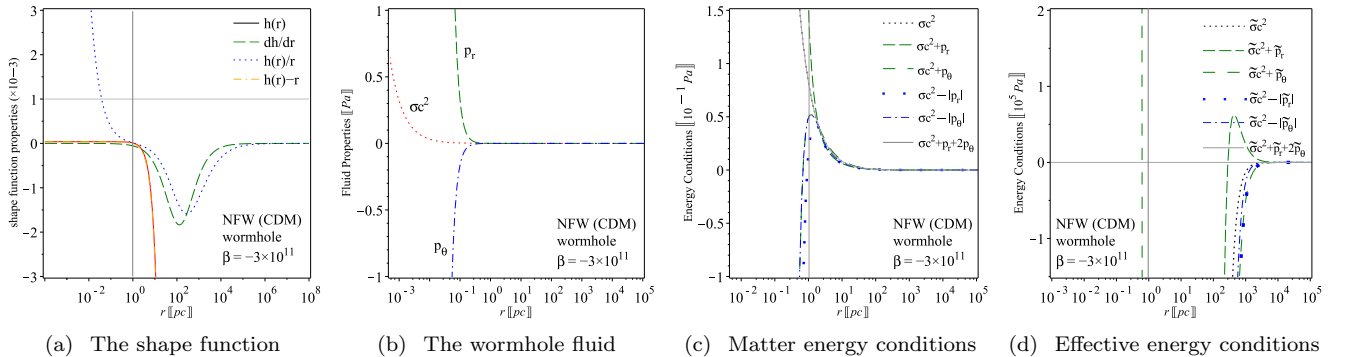


FIG. 10. Model II with large negative coupling $\beta \leq -1.842 \times 10^{11}$: (a) The wormhole is Lorentzian as $h(r) < r$ at $r > r_0$, additionally the flaring-out condition is fulfilled. (b) The matter fluid, the density has a flat profile at the core as suggested to solve the core-cusp problem with $p_r > 0$ and $p_\theta < 0$. (c) The matter energy conditions are fulfilled at $r > r_0$. (d) The effective energy conditions are broken at $r > r_0$ which represents the GR case. We set $r_0 = 1$ pc, for the galaxy NGC 2366, $\sigma_s = 3.11 \times 10^{-3} \text{ M}_\odot/\text{pc}^3$ and $r_s = 1.447$ kpc [62].

In conclusion, the above calculations confirm the possibility to find a healthy wormhole solution where the energy conditions are broken only on the effective sector but satisfied on the matter sector. Consequently, no exotic matter is needed to form a physical wormhole as required in the GR framework, if non-minimal coupling between matter and geometry has been considered.

VII. STABILITY OF THE WORMHOLE SOLUTIONS

In this section, we investigate the stability of the obtained wormhole solutions. Stability is often verified using hydrostatic equilibrium constraints, known as the Tolman-Oppenheimer-Volkoff (TOV) equation [69–71], showing that these wormholes can be dynamically stable. Recalling the field equations (19), which show that the conservation is no longer hold on the matter sector $\nabla_\mu \mathcal{T}^\mu_\nu \neq 0$, since $\nabla_\mu \mathcal{T}^\mu_\nu^{(\text{NMG})} \neq 0$. However, the total (effective) stress-energy tensor satisfies $\nabla_\mu \tilde{\mathcal{T}}^\mu_\nu = 0$ as required by applying Bianchi identity to the left hand side of the field equations. This modifies TOV equation introducing a new force due to non-minimal coupling between matter and geometry. For the present theory, $f(\mathcal{Q}, \mathcal{T}) = \mathcal{Q} + \beta\mathcal{T}$, we write the following modified TOV equation:

$$p'_r = -\frac{3(1+2\beta)(\sigma c^2 + p_r)}{3+7\beta}\xi' + \beta\frac{3\sigma' c^2 - 2p'_\theta}{3+7\beta} + \frac{6(1+2\beta)(p_\theta - p_r)}{(3+7\beta)r}. \quad (65)$$

Then, we define the contributing forces in the above equation, where the hydrostatic, gravitational, coupling and anisotropic forces are respectively given as

$$F_h = -p'_r, \quad F_g = -\frac{3(1+2\beta)(\sigma c^2 + p_r)}{3+7\beta}\xi', \quad F_c = \beta\frac{3\sigma' c^2 - 2p'_\theta}{3+7\beta}, \quad F_a = \frac{6(1+2\beta)(p_\theta - p_r)}{(3+7\beta)r}. \quad (66)$$

Clearly, by setting the non-minimal coupling coefficient $\beta = 0$, the coupling force F_c vanishes, and the above hydrostatic equilibrium equation reduces to the GR version

$$p'_r = -(\sigma c^2 + p_r)\xi' + \frac{2}{r}(p_\theta - p_r).$$

In order for the wormhole solutions to be stable, the sum of the forces F_h , F_g , F_c and F_a should be zero. Given the redshift function $\xi(r) = \xi_0 = \text{constant}$ as is assumed in this study, there is no tidal force $\mathcal{F}_g = 0$, resulting in the stability constraint being reformulated as:

$$F_h + F_c + F_a = 0. \quad (67)$$

We note that the coefficient of the anisotropic force in Eq. (66), i.e. $\frac{1+2\beta}{3+7\beta} = \frac{2}{7} + \frac{1}{7(3+7\beta)} \rightarrow \frac{2}{7}$ for large $|\beta|$, in addition it is always positive as $\beta < -1/2$ as required by the NEC. In this case, the anisotropic force could be repulsive (attractive) when $p_r < p_\theta$ ($p_r > p_\theta$). For the wormhole solution, assuming $f(\mathcal{Q}, \mathcal{T}) = \mathcal{Q} + \beta\mathcal{T}$ with $\xi(r) = \xi_0$, the forces can be written in terms of the shape function as

$$F_h = -\frac{3h}{(1+2\beta)\kappa^2 r^4} + \frac{(3+20\beta)h'}{3(1+2\beta)(1+4\beta)\kappa^2 r^3} - \frac{4\beta h''}{3(1+2\beta)(1+4\beta)\kappa^2 r^2}, \quad (68)$$

$$F_c = \frac{3\beta h}{(1+2\beta)(3+7\beta)\kappa^2 r^4} - \frac{\beta(27+68\beta)h'}{3(1+2\beta)(1+4\beta)(3+7\beta)\kappa^2 r^3} + \frac{4\beta h''}{3(1+2\beta)(1+4\beta)\kappa^2 r^2}, \quad (69)$$

$$F_a = \frac{9h}{(3+7\beta)\kappa^2 r^4} - \frac{3h'}{(3+7\beta)\kappa^2 r^3}. \quad (70)$$

One can easily fulfill the hydrostatic equilibrium constraint, namely (67), by virtue of the above equations.

A. Model I

For soliton model of DM, we insert the shape function (44) into Eqs (68)–(70), which derives the corresponding forces

$$\begin{aligned}
F_h = & \frac{3}{(1+2\beta)\kappa^2 r^4} \left[r_0 + A \left[\arctan(\sqrt{\alpha}r/r_c) - \arctan(\sqrt{\alpha}r_0/r_c) \right] + B \frac{r-r_0}{(r_c^2 + \alpha r^2)^7} \mathcal{F}(r) \right] \\
& + \frac{(3+20\beta)}{3(1+2\beta)(1+4\beta)\kappa^2 r^3} \left[\frac{A\sqrt{\alpha}}{r_c \left(1 + \frac{r^2\alpha}{r_c^2}\right)} + \frac{\mathcal{F}'(r)(r-r_0)}{(r_c^2 + r^2\alpha)^7} + \frac{\mathcal{F}(r)}{(r_c^2 + r^2\alpha)^7} - 14 \frac{\mathcal{F}(r)(r-r_0)r\alpha}{(r_c^2 + r^2\alpha)^8} \right] \\
& - \frac{4\beta}{3(1+2\beta)(1+4\beta)\kappa^2 r^2} \left[-\frac{2A\alpha^{3/2}r}{r_c^3 \left(1 + \frac{r^2\alpha}{r_c^2}\right)^2} + \frac{\mathcal{F}''(r)(r-r_0)}{(r_c^2 + r^2\alpha)^7} + \frac{2\mathcal{F}'(r)}{(r_c^2 + r^2\alpha)^7} - \frac{28\mathcal{F}'(r)(r-r_0)r\alpha}{(r_c^2 + r^2\alpha)^8} \right. \\
& \left. - \frac{28\mathcal{F}(r)r\alpha}{(r_c^2 + r^2\alpha)^8} + \frac{224\mathcal{F}(r)(r-r_0)r^2\alpha^2}{(r_c^2 + r^2\alpha)^9} - \frac{14\mathcal{F}(r)(r-r_0)\alpha}{(r_c^2 + r^2\alpha)^8} \right], \tag{71}
\end{aligned}$$

$$\begin{aligned}
F_c = & \frac{3\beta}{(1+2\beta)(3+7\beta)\kappa^2 r^4} \left[r_0 + A \left[\arctan(\sqrt{\alpha}r/r_c) - \arctan(\sqrt{\alpha}r_0/r_c) \right] + B \frac{r-r_0}{(r_c^2 + \alpha r^2)^7} \mathcal{F}(r) \right] \\
& - \frac{\beta(27+68\beta)}{3(1+2\beta)(1+4\beta)(3+7\beta)\kappa^2 r^3} \left[\frac{A\sqrt{\alpha}}{r_c \left(1 + \frac{r^2\alpha}{r_c^2}\right)} + \frac{\mathcal{F}'(r)(r-r_0)}{(r_c^2 + r^2\alpha)^7} + \frac{\mathcal{F}(r)}{(r_c^2 + r^2\alpha)^7} - 14 \frac{\mathcal{F}(r)(r-r_0)r\alpha}{(r_c^2 + r^2\alpha)^8} \right] \\
& + \frac{4\beta}{3(1+2\beta)(1+4\beta)\kappa^2 r^2} \left[-\frac{2A\alpha^{3/2}r}{r_c^3 \left(1 + \frac{r^2\alpha}{r_c^2}\right)^2} + \frac{\mathcal{F}''(r)(r-r_0)}{(r_c^2 + r^2\alpha)^7} + \frac{2\mathcal{F}'(r)}{(r_c^2 + r^2\alpha)^7} - \frac{28\mathcal{F}'(r)(r-r_0)r\alpha}{(r_c^2 + r^2\alpha)^8} \right. \\
& \left. - \frac{28\mathcal{F}(r)r\alpha}{(r_c^2 + r^2\alpha)^8} + \frac{224\mathcal{F}(r)(r-r_0)r^2\alpha^2}{(r_c^2 + r^2\alpha)^9} - \frac{14\mathcal{F}(r)(r-r_0)\alpha}{(r_c^2 + r^2\alpha)^8} \right], \tag{72}
\end{aligned}$$

(73)

$$\begin{aligned}
F_a = & \frac{9}{(3+7\beta)\kappa^2 r^4} \left[r_0 + A \left[\arctan(\sqrt{\alpha}r/r_c) - \arctan(\sqrt{\alpha}r_0/r_c) \right] + B \frac{r-r_0}{(r_c^2 + \alpha r^2)^7} \mathcal{F}(r) \right] \\
& - \frac{3}{(3+7\beta)\kappa^2 r^3} \left[\frac{A\sqrt{\alpha}}{r_c \left(1 + \frac{r^2\alpha}{r_c^2}\right)} + \frac{\mathcal{F}'(r)(r-r_0)}{(r_c^2 + r^2\alpha)^7} + \frac{\mathcal{F}(r)}{(r_c^2 + r^2\alpha)^7} - 14 \frac{\mathcal{F}(r)(r-r_0)r\alpha}{(r_c^2 + r^2\alpha)^8} \right]. \tag{74}
\end{aligned}$$

We plot the above mentioned forces for the galaxy NGC 2366, setting $r_0 = 1$ pc, $\sigma_c = 15 \times 10^{-3} M_\odot/\text{pc}^3$ and $r_c = 3$ kpc, for three different values of the non-minimal coupling parameter β as seen in Fig. 11. (i) For $\beta = -0.6 < -1/2$, see Fig. 11(a), which is consistent with the flaring-out in addition to the NEC, the repulsive hydrostatic force $F_h > 0$ is compensated by other two attractive forces, those are the anisotropic force $F_a < 0$ (i.e. $p_r > p_\theta$) in addition to the coupling force F_c which is attractive in this case. (ii) For $\beta \geq 1.840 \times 10^{13}$, see Fig. 11(b), which satisfies all the energy conditions but breaks the flaring-out condition, the anisotropic force is repulsive (i.e. $p_r > p_\theta$) and balanced by the other two forces, the hydrostatic force and the force due to the non-minimal coupling between matter and geometry, those are interpolating between attractive and repulsive behavior at different radial distance $r > r_0$. However, the resultant force is null in all distances. (iii) For $\beta \leq -5.519 \times 10^{13}$, see Fig. 11(c), similar to large positive β case, but it satisfies all the energy conditions in addition to the flaring-out condition.

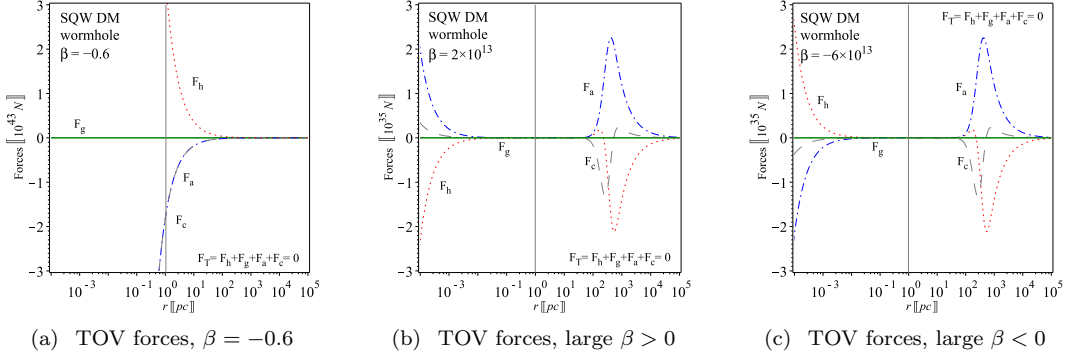


FIG. 11. Model I constituent forces of the modified TOV equation (65). The absence of the gravitational force is due to our choice of the redshift function $\xi(r) = \xi_0$, while other constituent forces F_h , F_c and F_a as given by (71)–(74). (a) For $\beta = -0.6 < -1/2$, which is consistent with the flaring-out in addition to the NEC, the repulsive hydrostatic force $F_h > 0$ is compensated by other two attractive forces, those are the anisotropic force $F_a < 0$ (i.e. $p_r > p_\theta$) in addition to the coupling force F_c which is attractive in this case. (b) For $\beta \geq 1.840 \times 10^{13}$, which satisfies all the energy conditions but breaks the flaring-out condition, the anisotropic force is repulsive (i.e. $p_r > p_\theta$) and balanced by the other two forces, the hydrostatic force and the force due to the non-minimal coupling between matter and geometry, those are interpolating between attractive and repulsive behavior at different radial distance $r > r_0$. However, the resultant force is null in all distances. (c) For $\beta \leq -5.519 \times 10^{13}$, similar to large positive β case, but it satisfies all the energy conditions in addition to the flaring-out condition. We set $r_0 = 1$ pc, for the galaxy NGC 2366, where $\sigma_c = 15 \times 10^{-3} M_\odot/\text{pc}^3$ and $r_c = 3$ kpc [62].

B. Model II

For NFW model of DM, we insert the shape function (52) into Eqs (68)–(70), which derives the corresponding forces

$$F_h = \frac{3}{(1+2\beta)\kappa^2 r^4} \left[r_0 + \frac{\tilde{A}(r-r_0)}{r+r_s} + \tilde{B} \ln \left(\frac{r+r_s}{r_s+r_0} \right) \right] + \frac{(3+20\beta) \left[\tilde{B}r + (\tilde{A} + \tilde{B})r_s + \tilde{A}r_0 \right]}{3(r+r_s)^2(1+2\beta)(1+4\beta)\kappa^2 r^3} + \frac{4\beta \left[\tilde{B}r + (2\tilde{A} + \tilde{B})r_s + 2\tilde{A}r_0 \right]}{3(r+r_s)^3(1+2\beta)(1+4\beta)(3+7\eta)\kappa^2 r^2}, \quad (75)$$

$$F_c = \frac{3\beta}{(1+2\beta)(3+7\beta)\kappa^2 r^4} \left[r_0 + \tilde{A} \frac{r-r_0}{r_s+r} + \tilde{B} \ln \left(\frac{r_s+r}{r_s+r_0} \right) \right] - \frac{\beta(27+68\beta)}{3(1+2\beta)(1+4\beta)(3+7\beta)\kappa^2 r^3} \times \left[\frac{(\tilde{A} + \tilde{B})r_s + \tilde{A}r_0 + \tilde{B}r}{(r+r_s)^2} \right] - \frac{4\beta}{3(1+2\beta)(1+4\beta)\kappa^2 r^2} \left[\frac{(2\tilde{A} + \tilde{B})r_s + 2\tilde{A}r_0 + \tilde{B}r}{(r+r_s)^3} \right], \quad (76)$$

$$F_a = \frac{9}{(3+7\beta)\kappa^2 r^4} \left[r_0 + \frac{\tilde{A}(r-r_0)}{r+r_s} + \tilde{B} \ln \left(\frac{r+r_s}{r_s+r_0} \right) \right] - \frac{(3\tilde{A} + 3\tilde{B})r_s + 3\tilde{A}r_0 + 3\tilde{B}r}{(r+r_s)^2(3+7\beta)\kappa^2 r^3}. \quad (77)$$

We plot the above mentioned forces for the galaxy NGC 2366, setting $r_0 = 1$ pc, $\sigma_s = 3.11 \times 10^{-3} M_\odot/\text{pc}^3$ and $r_s = 1.447$ kpc, for three different values of the non-minimal coupling parameter β as seen in Fig. 12. (i) For $\beta = -0.6 < -1/2$, see Fig. 12(a), which is consistent with the flaring-out in addition to the NEC, the repulsive hydrostatic force $F_h > 0$ is compensated by other two attractive forces, those are the anisotropic force $F_a < 0$ (i.e. $p_r > p_\theta$) in addition to the coupling force F_c which is attractive in this case. (ii) For $\beta \geq 6.140 \times 10^{10}$, see Fig. 12(b), which satisfies all the energy conditions but breaks the flaring-out condition, the anisotropic force is repulsive (i.e. $p_r > p_\theta$) and balanced by the other two forces, the hydrostatic force and the force due to the non-minimal coupling between matter and geometry, those are interpolating between attractive and repulsive behavior at different radial distance $r > r_0$. However, the resultant force is null in all distances. (iii) For $\beta \leq -1.842 \times 10^{11}$, see Fig. 12(c), similar to large positive β case, but it satisfies all the energy conditions in addition to the flaring-out condition.

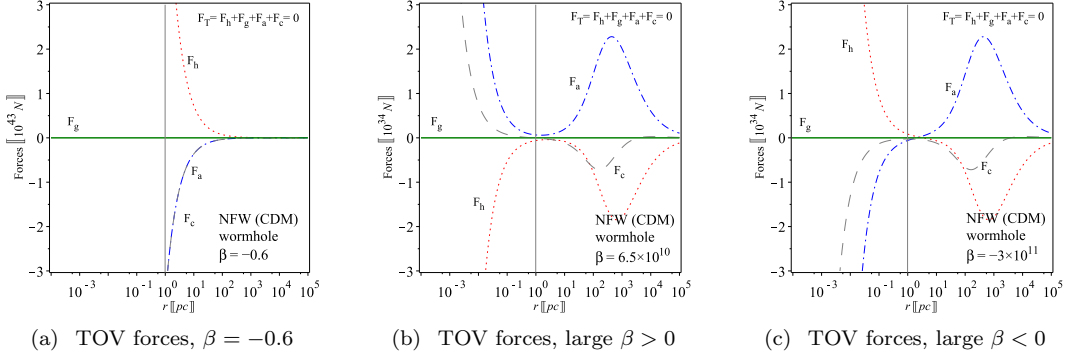


FIG. 12. Model II constituent forces of the modified TOV equation (65). The absence of the gravitational force is due to our choice of the redshift function $\xi(r) = \xi_0$, while constituent forces F_h , F_c and F_a as given by (75)–(77). (a) For $\beta = -0.6 < -1/2$, which is consistent with the flaring-out in addition to the NEC, the repulsive hydrostatic force $F_h > 0$ is compensated by the attractive anisotropic force $F_a < 0$ (i.e. $p_r > p_\theta$) in addition to the coupling force F_c which is attractive in this case. (b) For $\beta \geq 6.140 \times 10^{10}$, which satisfies all the energy conditions but breaks the flaring-out condition, the anisotropic force is repulsive (i.e. $p_r > p_\theta$) and balanced by the other two forces, the hydrostatic force and the force due to the non-minimal coupling between matter and geometry, those are interpolating between attractive and repulsive behavior at different radial distance $r > r_0$. However, the resultant force is null in all distances. (c) For $\beta \leq -1.842 \times 10^{11}$, similar to large positive β case, but it satisfies all the energy conditions in addition to the flaring-out condition. We set $r_0 = 1$ pc, for the galaxy NGC 2366, $\sigma_s = 3.11 \times 10^{-3} \text{ M}_\odot/\text{pc}^3$ and $r_s = 1.447$ kpc [62].

VIII. SUMMARY AND CONCLUSION

In this study, we have explored wormhole models within the framework of the linear form of $f(\mathcal{Q}, \mathcal{T})$ gravity. By adopting a spherically symmetric and static spacetime in the presence of anisotropic matter, we derived the field equations that govern the structure of wormholes, with a particular focus on linear $f(\mathcal{Q}, \mathcal{T}) = \mathcal{Q} + \beta\mathcal{T}$ gravity, where GR is recovered by setting $\beta = 0$. In the GR context, the flaring-out condition, which plays a fundamental role in wormhole physics, necessarily violates the NEC. Therefore, the price to have a wormhole in GR is the existence of exotic matter. However, in a different context, as in modified gravity, which accounts for non-minimal coupling between matter and geometry, we may obtain different results. This was the aim of the present study.

It has been shown that DM could be consistent with wormhole structure at galactic halos [58, 59] and even at the central regions [60]. In the present study, we used Soliton+NFW DM density profile to derive the corresponding shape functions, where soliton model is applied at the galactic core region and the NFW model is applied at the outer regions of the galactic halo of the dwarf galaxy NGC 2366. We use the model parameters for the two models as appear in [62]: Model I (soliton), the dwarf galaxy NGC 2366 core radius is $r_c = 3$ kpc and the central density is $\sigma_c = 15 \times 10^{-3} \text{ M}_\odot/\text{pc}^3$. Model II (NFW), the dwarf galaxy NGC 2366 scale radius is $r_s = 1.447$ kpc and the corresponding scale density is $\sigma_s = 3.11 \times 10^{-3} \text{ M}_\odot/\text{pc}^3$.

Recalling the flaring-out condition at the wormhole throat, we found the following constraints on the coupling strength: In model I, we obtained the viable parameter space $\{\beta, r_0\}$ for an arbitrary throat size r_0 as given by Eqs. (47) and (48), and by setting $r_0 = 1$ pc, these give $\beta < -3/8 - 8.494 \times 10^{-16}$ or $-3/8 < \beta < 1.840 \times 10^{13}$. In model II, similarly, we obtained the viable parameter space $\{\beta, r_0\}$ as given by Eqs. (54) and (55), and by setting $r_0 = 1$ pc, these give $\beta < -3/8 - 2.545 \times 10^{-13}$ or $-3/8 < \beta < 6.140 \times 10^{10}$. In general, for the corresponding valid regions of the coupling parameter β , the wormhole models fulfill the following constraints:

- (i) At the throat $r = r_0$; the shape function $h(r_0) = r_0$, $h'(r_0) < 1$, $z(r_0) = 0$ and $z'(r_0) \rightarrow \infty$.
- (ii) At finite radius $r > r_0$; the shape function $h(r) < r$, $h'(r) < 1$, $z(r)$ is finite and $z'(r)$ is finite.
- (iii) At infinite distance from the wormhole $r \rightarrow \infty$; the shape function satisfies $h(r)/r \rightarrow 0$, $h'(r) \rightarrow 0$, $z(r) \rightarrow \pm\infty$ and $z'(r) \rightarrow 0$.

Interestingly, we have shown that the flaring-out condition can be reconciled with the NEC in the context of $f(\mathcal{Q}, \mathcal{T})$ modified gravity. More precise, one must violate the NEC only effectively when the flaring-out condition holds. However, for the matter sector, one could have $\sigma c^2 + p_r > 0$ where $\beta < -1/2$, which is not recovered in the GR regime, and therefore the NEC is fulfilled. In this case, the NEC condition is broken only effectively, whereas the matter sector preserves the NEC with no need for exotic matter. We remark that $\beta < -1/2$ is consistent with our findings by applying the flaring-out condition.

In addition, we have shown that all energy conditions can be satisfied for certain bounds on the strength of the matter-geometry non-minimal coupling: For model I, with $r_0 = 1$ pc, we found the following constraints $|\beta| \gtrsim 10^{13}$, while for the same r_0 , the faring-out condition excludes exactly the positive coupling. Similarly, for model II, with $r_0 = 1$ pc, the energy conditions set the following constraints $|\beta| \gtrsim 10^{11}$, while the faring-out condition excludes exactly the positive solution. In general, for large positive coupling parameter, the null energy condition (NEC) among other energy conditions, can be satisfied at the wormhole throat, meaning exotic matter is not needed, while the wormhole is no longer Lorentzian and the flaring-out condition is broken. However, for large negative coupling parameters, the NEC among other conditions, can be satisfied, allowing for healthy wormholes without exotic matter, provided the coupling strength stays within certain bounds. In the latter case, the NEC is broken only effectively.

The $f(Q, T)$ theory modifies gravity considering possible non-minimal between matter and geometry, this requires breaking of matter conservation. Nevertheless, the matter-geometry coupling compensates for it by additional non-conservative sector holds the conservation law effectively. In this sense, the new coupling term contributes by adding extra force to the hydrostatic equilibrium equation, known as TOV equation. We investigated the stability of both wormhole models by virtue of a modified version of TOV equation, which includes a new force due to matter-geometry non-minimal, showing that these wormholes are dynamically stable.

In conclusion, the present study confirms the possibility to find a healthy wormhole solution where the energy conditions are broken only on the effective sector but satisfied on the matter sector. Consequently, no exotic matter is needed to form a physical wormhole as required in the GR framework, if non-minimal coupling between matter and geometry has been considered.

[1] E. Gourgoulhon, A. Le Tiec, F. H. Vincent, and N. Warburton, *Astron. Astrophys.* **627**, A92 (2019), [arXiv:1903.02049 \[gr-qc\]](https://arxiv.org/abs/1903.02049).

[2] A. A. Chael, M. D. Johnson, R. Narayan, S. S. Doebleman, J. F. C. Wardle, and K. L. Bouman, *The Astrophysical Journal* **829**, 11 (2016).

[3] K. Akiyama *et al.* (Event Horizon Telescope), *Astrophys. J. Lett.* **875**, L1 (2019), [arXiv:1906.11238 \[astro-ph.GA\]](https://arxiv.org/abs/1906.11238).

[4] C. Winkler *et al.*, *Astron. Astrophys.* **411**, L1 (2003).

[5] R. Abuter *et al.* (GRAVITY), *Astron. Astrophys.* **636**, L5 (2020), [arXiv:2004.07187 \[astro-ph.GA\]](https://arxiv.org/abs/2004.07187).

[6] X. Barcons, D. Barret, A. Decourchelle, J. W. den Herder, A. C. Fabian, H. Matsumoto, D. Lumb, K. Nandra, L. Piro, R. K. Smith, and R. Willingale, *Astronomische Nachrichten* **338**, 153 (2017).

[7] P. Soffitta *et al.*, *Exper. Astron.* **36**, 523 (2013), [arXiv:1309.6995 \[astro-ph.HE\]](https://arxiv.org/abs/1309.6995).

[8] D. N. Burrows *et al.* (SWIFT), *Space Sci. Rev.* **120**, 165 (2005), [arXiv:astro-ph/0508071](https://arxiv.org/abs/astro-ph/0508071).

[9] M. Amiri *et al.* (CHIME/FRB), (2018), 10.3847/1538-4357/aad188, [arXiv:1803.11235 \[astro-ph.IM\]](https://arxiv.org/abs/1803.11235).

[10] E. Abdalla *et al.*, *Astron. Astrophys.* **664**, A14 (2022), [arXiv:2107.01633 \[astro-ph.CO\]](https://arxiv.org/abs/2107.01633).

[11] P. J. Hall, *The Square Kilometre Array: An Engineering Perspective* (Springer Dordrecht, 2005).

[12] P. A. Seoane *et al.* (eLISA), (2013), [arXiv:1305.5720 \[astro-ph.CO\]](https://arxiv.org/abs/1305.5720).

[13] M. Visser, *Lorentzian wormholes: From Einstein to Hawking* (1995).

[14] P. Bueno, P. A. Cano, F. Goelen, T. Hertog, and B. Vercnocke, *Phys. Rev. D* **97**, 024040 (2018), [arXiv:1711.00391 \[gr-qc\]](https://arxiv.org/abs/1711.00391).

[15] S. Paul, R. Shaikh, P. Banerjee, and T. Sarkar, *JCAP* **03**, 055 (2020), [arXiv:1911.05525 \[gr-qc\]](https://arxiv.org/abs/1911.05525).

[16] A. Övgün, G. Gyulchev, and K. Jusufi, *Annals Phys.* **406**, 152 (2019), [arXiv:1806.03719 \[gr-qc\]](https://arxiv.org/abs/1806.03719).

[17] A. Övgün, *Phys. Rev. D* **98**, 044033 (2018), [arXiv:1805.06296 \[gr-qc\]](https://arxiv.org/abs/1805.06296).

[18] A. Övgün, *Turk. J. Phys.* **44**, 465 (2020), [arXiv:2011.04423 \[gr-qc\]](https://arxiv.org/abs/2011.04423).

[19] M. S. Morris and K. S. Thorne, *Am. J. Phys.* **56**, 395 (1988).

[20] J. Maldacena and A. Milekhin, *Phys. Rev. D* **103**, 066007 (2021), [arXiv:2008.06618 \[hep-th\]](https://arxiv.org/abs/2008.06618).

[21] L. Randall and R. Sundrum, *Phys. Rev. Lett.* **83**, 4690 (1999), [arXiv:hep-th/9906064](https://arxiv.org/abs/hep-th/9906064).

[22] M. Ilyas and K. Bamba, *JCAP* **10**, 038 (2023), [arXiv:2308.11004 \[gr-qc\]](https://arxiv.org/abs/2308.11004).

[23] H. A. Buchdahl, *Mon. Not. Roy. Astron. Soc.* **150**, 1 (1970).

[24] A. A. Starobinsky, *JETP Lett.* **30**, 682 (1979).

[25] A. De Felice and S. Tsujikawa, *Living Rev. Rel.* **13**, 3 (2010), [arXiv:1002.4928 \[gr-qc\]](https://arxiv.org/abs/1002.4928).

[26] T. P. Sotiriou and V. Faraoni, *Rev. Mod. Phys.* **82**, 451 (2010), [arXiv:0805.1726 \[gr-qc\]](https://arxiv.org/abs/0805.1726).

[27] S. Nojiri, S. D. Odintsov, and V. K. Oikonomou, *Phys. Rept.* **692**, 1 (2017), [arXiv:1705.11098 \[gr-qc\]](https://arxiv.org/abs/1705.11098).

[28] S. Nojiri and S. D. Odintsov, *Phys. Rept.* **505**, 59 (2011), [arXiv:1011.0544 \[gr-qc\]](https://arxiv.org/abs/1011.0544).

[29] S. Nojiri and S. D. Odintsov, *eConf* **C0602061**, 06 (2006), [arXiv:hep-th/0601213](https://arxiv.org/abs/hep-th/0601213).

[30] S. Capozziello and M. De Laurentis, *Annalen Phys.* **524**, 545 (2012).

[31] T. Harko, F. S. N. Lobo, S. Nojiri, and S. D. Odintsov, *Phys. Rev. D* **84**, 024020 (2011), [arXiv:1104.2669 \[gr-qc\]](https://arxiv.org/abs/1104.2669).

[32] G. Sardar, A. Bose, and S. Chakraborty, *Eur. Phys. J. C* **83**, 41 (2023).

[33] T. D. Pappas, C. Posada, and Z. Stuchlík, *Phys. Rev. D* **106**, 124014 (2022), [arXiv:2210.15597 \[gr-qc\]](https://arxiv.org/abs/2210.15597).

[34] A. Bose, G. Sardar, and S. Chakraborty, *Phys. Dark Univ.* **37**, 101087 (2022), [arXiv:2209.01415 \[gr-qc\]](https://arxiv.org/abs/2209.01415).

[35] P. H. R. S. Moraes and J. R. L. Santos, *Eur. Phys. J. C* **76**, 60 (2016), [arXiv:1601.02811 \[gr-qc\]](https://arxiv.org/abs/1601.02811).

[36] J. Beltrán Jiménez, L. Heisenberg, and T. Koivisto, *Phys. Rev. D* **98**, 044048 (2018), arXiv:1710.03116 [gr-qc].

[37] R. Lazkoz, F. S. N. Lobo, M. Ortiz-Baños, and V. Salzano, *Phys. Rev. D* **100**, 104027 (2019), arXiv:1907.13219 [gr-qc].

[38] R. Solanki, S. K. J. Pacif, A. Parida, and P. K. Sahoo, *Phys. Dark Univ.* **32**, 100820 (2021), arXiv:2105.00876 [gr-qc].

[39] R. Solanki, D. S. Rana, S. Mandal, and P. K. Sahoo, *Fortsch. Phys.* **71**, 2200202 (2023), arXiv:2211.03514 [gr-qc].

[40] S. Mandal, P. K. Sahoo, and J. R. L. Santos, *Phys. Rev. D* **102**, 024057 (2020), arXiv:2008.01563 [gr-qc].

[41] Z. Hassan, S. Ghosh, P. K. Sahoo, and K. Bamba, *Eur. Phys. J. C* **82**, 1116 (2022), arXiv:2207.09945 [gr-qc].

[42] Z. Hassan, S. Ghosh, P. K. Sahoo, and V. S. H. Rao, *Gen. Rel. Grav.* **55**, 90 (2023), arXiv:2209.02704 [gr-qc].

[43] Y. Xu, G. Li, T. Harko, and S.-D. Liang, *Eur. Phys. J. C* **79**, 708 (2019), arXiv:1908.04760 [gr-qc].

[44] S. Arora, J. R. L. Santos, and P. K. Sahoo, *Phys. Dark Univ.* **31**, 100790 (2021), arXiv:2009.00240 [gr-qc].

[45] M. Tayde, S. Ghosh, and P. K. Sahoo, *Chin. Phys. C* **47**, 075102 (2023), arXiv:2305.03362 [gr-qc].

[46] Y. Myrzakulov, O. Donmez, M. Koussour, D. Alizhanov, S. Bekchanov, and J. Rayimbaev, *Phys. Dark Univ.* **46**, 101614 (2024), arXiv:2408.04770 [astro-ph.CO].

[47] A. Hazarika, S. Arora, P. K. Sahoo, and T. Harko, (2024), arXiv:2407.00989 [gr-qc].

[48] H. R. Kausar, A. Majid, and B. Nadeem, *Eur. Phys. J. Plus* **140**, 157 (2025).

[49] S. Pradhan, S. K. Maurya, P. K. Sahoo, and G. Mustafa, *Fortsch. Phys.* **72**, 2400092 (2024), arXiv:2408.02051 [gr-qc].

[50] K. P. Das and U. Debnath, *Eur. Phys. J. C* **84**, 513 (2024).

[51] X.-h. Meng and Y.-b. Wang, *Eur. Phys. J. C* **71**, 1755 (2011), arXiv:1107.0629 [astro-ph.CO].

[52] S. Bahamonde, K. F. Dialektopoulos, C. Escamilla-Rivera, G. Farrugia, V. Gakis, M. Hendry, M. Hohmann, J. Levi Said, J. Mifsud, and E. Di Valentino, *Rept. Prog. Phys.* **86**, 026901 (2023), arXiv:2106.13793 [gr-qc].

[53] P. S. Letelier, *Phys. Rev. D* **22**, 807 (1980).

[54] D. Deb, B. Mukhopadhyay, and F. Weber, *Astrophys. J.* **922**, 149 (2021), arXiv:2108.12436 [astro-ph.HE].

[55] P. H. R. S. Moraes, R. A. C. Correa, and R. V. Lobato, *JCAP* **07**, 029 (2017), arXiv:1701.01028 [gr-qc].

[56] M. Tayde, Z. Hassan, P. K. Sahoo, and S. Gutti, *Chin. Phys. C* **46**, 115101 (2022), arXiv:2206.01184 [gr-qc].

[57] M. Tayde, J. R. L. Santos, J. N. Araujo, and P. K. Sahoo, *Eur. Phys. J. Plus* **138**, 539 (2023), arXiv:2212.07943 [gr-qc].

[58] F. Rahaman, P. K. F. Kuhfittig, S. Ray, and N. Islam, *Eur. Phys. J. C* **74**, 2750 (2014), arXiv:1307.1237 [gr-qc].

[59] S. Sarkar, N. Sarkar, S. Aktar, M. Sarkar, F. Rahaman, and A. K. Yadav, *New Astron.* **109**, 102183 (2024).

[60] F. Rahaman, P. Salucci, P. K. F. Kuhfittig, S. Ray, and M. Rahaman, *Annals Phys.* **350**, 561 (2014), arXiv:1501.00490 [physics.gen-ph].

[61] A. Pozo, T. Broadhurst, I. de Martino, T. Chiueh, G. F. Smoot, S. Bonoli, and R. Angulo, *Phys. Rev. D* **110**, 043534 (2024), arXiv:2010.10337 [astro-ph.GA].

[62] A. Bañares Hernández, A. Castillo, J. Martin Camalich, and G. Iorio, *Astron. Astrophys.* **676**, A63 (2023), arXiv:2304.05793 [astro-ph.GA].

[63] G. Iorio, F. Fraternali, C. Nipoti, E. Di Teodoro, J. I. Read, and G. Battaglia, *Mon. Not. Roy. Astron. Soc.* **466**, 4159 (2017), arXiv:1611.03865 [astro-ph.GA].

[64] H.-Y. Schive, T. Chiueh, and T. Broadhurst, *Nature Phys.* **10**, 496 (2014), arXiv:1406.6586 [astro-ph.GA].

[65] H.-Y. Schive, M.-H. Liao, T.-P. Woo, S.-K. Wong, T. Chiueh, T. Broadhurst, and W. Y. P. Hwang, *Phys. Rev. Lett.* **113**, 261302 (2014), arXiv:1407.7762 [astro-ph.GA].

[66] A. Herrera-Martín, M. Hendry, A. X. Gonzalez-Morales, and L. A. Ureña López, *Astrophys. J.* **872**, 11 (2019), arXiv:1707.09929 [astro-ph.CO].

[67] J. F. Navarro, C. S. Frenk, and S. D. M. White, *Astrophys. J.* **490**, 493 (1997), arXiv:astro-ph/9611107.

[68] A. Rueda and E. Contreras, *Phys. Rev. D* **111**, 044019 (2025), arXiv:2504.04854 [gr-qc].

[69] J. R. Oppenheimer and G. M. Volkoff, *Phys. Rev.* **55**, 374 (1939).

[70] V. Gorini, U. Moschella, A. Y. Kamenshchik, V. Pasquier, and A. A. Starobinsky, *Phys. Rev. D* **78**, 064064 (2008), arXiv:0807.2740 [astro-ph].

[71] P. K. F. Kuhfittig, *Fund. J. Mod. Phys.* **14**, 23 (2020), arXiv:2009.11179 [gr-qc].